JGR Planets

RESEARCH ARTICLE
10.1029/2020JE006372

Updated Perspectives and Hypotheses on the Mineralogy of Lower Mt. Sharp, Mars, as Seen From Orbit

Rachel Y. Sheppard[1], Ralph E. Milliken[1], Mario Parente[2], and Yuki Itoh[2]

[1]Department of Earth, Environmental and Planetary Sciences, Brown University, Providence, RI, USA, [2]Department of Electrical and Computer Engineering, University of Massachusetts, Amherst, MA, USA

Abstract Previous studies have shown that Mt. Sharp has stratigraphic variation in mineralogy that may record a global transition from a climate more conducive to clay mineral formation to one marked by increased sulfate production. To better understand how small-scale observations along the traverse path of NASA's Curiosity rover might be linked to such large-scale processes, it is necessary to understand the extent to which mineral signatures observed from orbit vary laterally and vertically. This study uses newly processed visible-shortwave infrared Compact Reconnaissance Imaging Spectrometer for Mars data and corresponding visible images to reexamine the mineralogy of lower Mt. Sharp, map mineral distribution, and evaluate stratigraphic relationships. We demonstrate the presence of darker-toned strata that appears to be throughgoing with spectral signatures of monohydrated sulfate. Strata above and below this zone are lighter-toned and contain polyhydrated sulfate and variable distribution of Fe/Mg clay minerals. Clay minerals are observed at multiple stratigraphic positions; unlike the kieserite zone these units cannot be traced laterally across Mt. Sharp. The kieserite zone appears to be stratigraphically confined, but in most locations the orbital data do not provide sufficient detail to determine whether mineral signatures conform to or cut across stratigraphic boundaries, leaving open the question as to whether the clay minerals and sulfates occur as detrital, primary chemical precipitates, and/or diagenetic phases. Future observations along Curiosity's traverse will help distinguish between these possibilities. Rover observations of clay-bearing strata in northwest Mt. Sharp may be more reflective of local conditions that could be distinct from those associated with other clay-bearing strata.

Plain Language Summary We use newly processed satellite spectral data to map the mineralogy of portions of Gale crater that have been previously difficult to analyze conclusively. We find that a monohydrated Mg sulfate area appears to be stratigraphically restricted and run through the entirety of Mt. Sharp. Clay mineral and polyhydrated Mg sulfate signatures, however, are found in a wide range of stratigraphic positions. We present testable hypotheses for the formation of these mineral signatures that the rover will be able to address as it approaches these areas rich in hydrous minerals in the coming years.

Key Points:

- New methods allow for significant denoising of Compact Reconnaissance Imaging Spectrometer for Mars data and conclusive spectral analysis of regions previously too noisy to map
- A dark-toned section of strata in Mt. Sharp appears to be throughgoing and exhibits spectral signatures of monohydrated sulfate
- Clay minerals are observed at multiple stratigraphic positions throughout Mt. Sharp and cannot be traced laterally across the mountain

Correspondence to:
R. Y. Sheppard,
rachelysheppard@gmail.com

Citation:
Sheppard, R. Y., Milliken, R. E., Parente, M., & Itoh, Y. (2020). Updated perspectives and hypotheses on the mineralogy of lower Mt. Sharp, Mars, as seen from orbit. *Journal of Geophysical Research: Planets*, *126*, e2020JE006372. https://doi.org/10.1029/2020JE006372

Received 8 JAN 2020
Accepted 7 OCT 2020

1. Introduction

Gale crater is a ~155 km diameter impact crater that is situated along the martian dichotomy boundary and that is currently being explored in situ by NASA's Mars Science Laboratory rover, Curiosity (Figure 1). A dominant feature in Gale is its asymmetric central mountain, Mt. Sharp (later formally named Aeolis Mons), that rises ~5.5 km above the bottom of the modern crater floor (Grotzinger et al., 2012). A primary motivation for selecting Gale crater as a landing site was the orbital observation of a diversity of features in visible and thermal infrared data as well as distinct changes in mineralogy with elevation (stratigraphic height) (Anderson & Bell, 2010; Malin & Edgett, 2000; Milliken et al., 2010; Pelkey & Jakosky, 2002, 2004; Thomson et al., 2011). Based on these observations, the strata of Mt. Sharp may record a wide range of ancient depositional environments in a well-preserved stratigraphic sequence (Grotzinger et al., 2015). However, the specific modes of deposition are not clear based solely on orbital data. Although the observation of laterally continuous layers over tens of kilometers is consistent with a sedimentary origin (Anderson & Bell, 2010; Cabrol et al., 1999; Malin & Edgett, 2000; Thomson et al., 2011), the large-scale depositional environments and processes that formed the majority of Mt. Sharp, which has not been observed in situ, remains ambiguous. Rover-scale observations are thus necessary to accurately interpret what the diversity seen from orbit means in terms of the geologic history and evolution of Gale crater and the deposits therein.

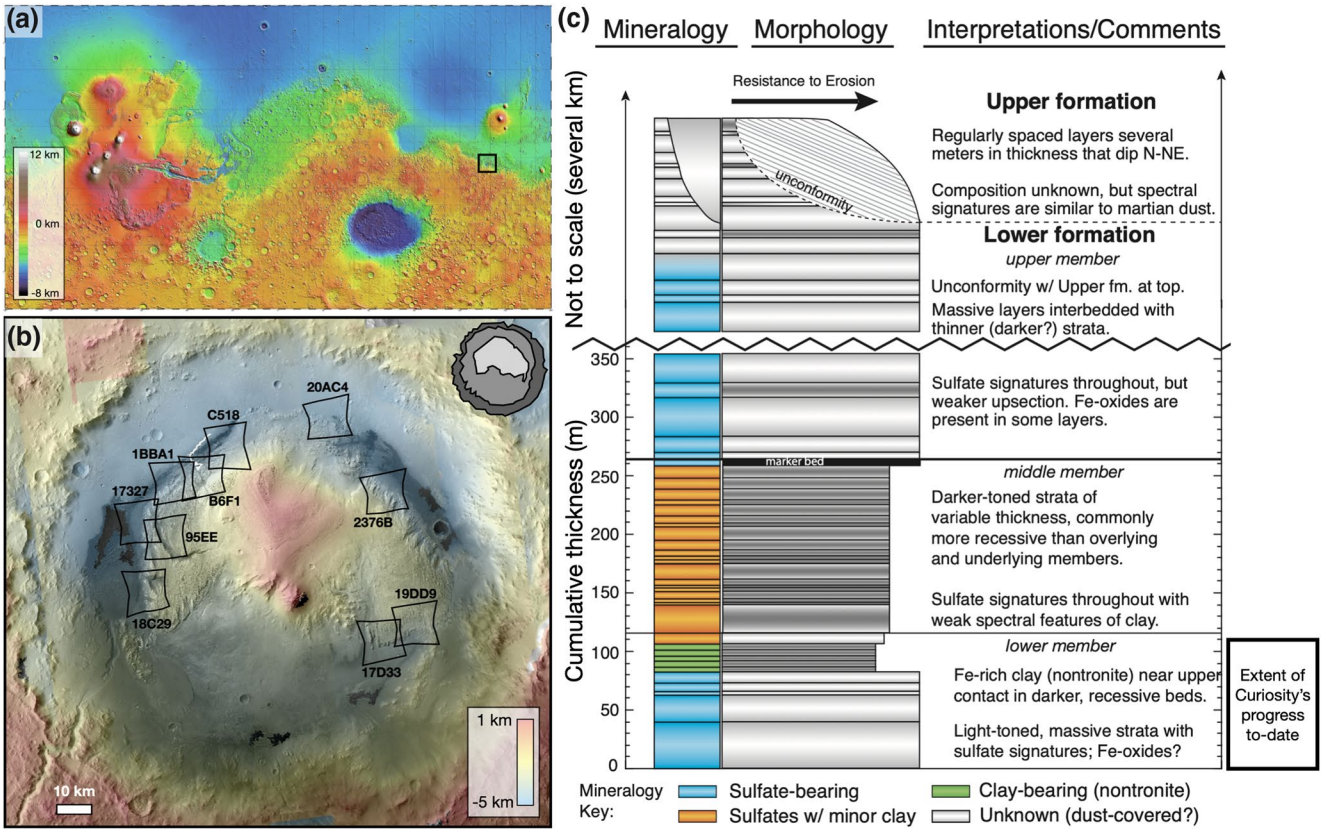

Figure 1. (a) Elevation from the Mars Orbiter Laser Altimeter instrument with the location of Gale crater. (b) Gale crater elevation (color) overlain on a Context Camera mosaic of Gale crater, with the planned rover traverse route (including planned Extended Mission 3 route) in white and outlines of the Compact Reconnaissance Imaging Spectrometer for Mars images used in this work outlined and labeled. The schematic in the top right shows the outline of Mt. Sharp in the crater and will be used throughout the paper to show the location of data being used for analysis. (c) The interpreted stratigraphic column reproduced from Milliken et al. (2010), for reference. The approximate span of the stratigraphic column explored by Curiosity to-date is marked on the bottom right.

Curiosity landed in Gale crater in 2012 has been ascending Mt. Sharp since 2014, collecting detailed measurements that allow orbital observations to be linked to specific geologic processes and environmental conditions. It is now clear that the lowermost strata of Mt. Sharp and the uppermost rocks of the crater floor to the north of those strata were deposited in an ancient alluvial-fluvial-lacustrine system (Grotzinger et al., 2015). However, to date the rover has only explored a small portion of the strata in lower Mt. Sharp that exhibit orbital evidence for hydrous minerals. Though in the future the rover will traverse additional clay mineral and sulfate-bearing strata, the total region explored by Curiosity will remain but a small fraction of Mt. Sharp. It has been suggested that the change from clay-bearing to sulfate-bearing to anhydrous mineral assemblages observed in orbital data of Gale may be a microcosm of martian climatic evolution (Milliken et al., 2010) recorded in secondary/alteration minerals at a global scale (Bibring et al., 2006). In order to test this hypothesis, and to aid in planning the future rover traverse route, it is important to understand whether or not local scale rover observations and characteristics observed along the traverse path are or are not representative of features observed elsewhere in Mt. Sharp. To provide a foundation for addressing this issue, this study presents an updated view of the mineralogy and selected morphologic/albedo characteristics of Mt. Sharp to better understand how existing and future rover observations can be linked to characteristics observed over larger (orbital) spatial scales.

We focus on the lateral and vertical distribution of hydrous minerals, clay minerals and sulfate salts in particular, to provide a more detailed assessment of their variations within the stratigraphy of lower Mt. Sharp. New methods for processing orbital near-infrared reflectance data, increased data coverage, and high resolution digital terrain models allow for refined mapping of the mineralogical stratigraphy of Mt.

Sharp along the northwestern (rover traverse), northeastern, southeastern, and western regions. Using the orbitally based stratigraphic column of Milliken et al. (2010) as a framework, we identify and evaluate several mineralogical and morphological characteristics that are common throughout Mt. Sharp, describe the extent to which these characteristics are expressed in the rover traverse region, and discuss how hypotheses for their origin may be tested by Curiosity's payload.

2. Background

2.1. Orbital Perspectives on Mt. Sharp

The strata of Mt. Sharp have previously been divided into a Lower and Upper formation that are separated by an erosional unconformity (Malin & Edgett, 2000; Milliken et al., 2010; Thomson et al., 2011). For the purpose of this study, and because our main focus is on the large scale mineralogical stratigraphy of Mt. Sharp, we adopt the stratigraphic framework of Milliken et al. (2010) that was based on visible High Resolution Imaging Science Experiment (HiRISE) data (McEwen et al., 2007) and high spectral resolution visible-shortwave infrared Compact Reconnaissance Imaging Spectrometer for Mars (CRISM) reflectance data (Murchie et al., 2007). We adopt this system here for two reasons: it is dominantly based on mineralogy rather than geomorphology, and it was constructed based on the stratigraphy of the northwest of Mt. Sharp where we now have rover data to add ground truthing. Furthermore, it is important to emphasize that this scheme is based on orbital analyses, dividing the stratigraphy into orbital formations. These are therefore based on relatively broad features compared to formations described in situ by the rover (e.g., the Murray formation) where finer scale evidence for changes in depositional environment can be used. The orbital Lower, Middle, and Upper formations used as the framework here are extremely broad and based on integration of spectral and HiRISE data and may or may not correlate to how formation boundaries will be observed by the rover.

In this scheme (Figure 1c), the Lower formation is divided into three members; the transition from lower member to middle member is marked by a distinct transition from lighter-toned massive strata to darker-toned recessive strata of variable thickness; the transition from middle member to upper member is marked by a return to lighter-toned massive strata and by the presence of an enigmatic dark "marker bed," with the marker bed representing the upper boundary of the middle member. The upper member of the Lower formation continues upsection to the unconformity that marks the boundary between the Lower and Upper formations. The changes in tonality associated with the three members of the Lower formation are relatively continuous and distinct along the western and northwestern faces of Mt. Sharp (Milliken et al., 2010). Notably, orbital reflectance spectra of the Lower formation indicate it hosts clay minerals and hydrated sulfates, whereas such signatures are lacking in reflectance spectra of the Upper formation.

A range of depositional environments have been proposed to explain the emplacement of strata of the Lower formation (Anderson & Bell, 2010; Cabrol et al., 1999; Kite et al., 2013; Le Deit et al., 2013; Rossi et al., 2008; Thomson et al., 2011; Wray, 2013), but ultimately the mode of deposition is ambiguous from orbital data alone. Crater retention ages indicate the Lower formation was likely deposited in the Late Noachian to Early Hesperian (~3.6–3.4 Ga) (Thomson et al., 2011), and the observation that it is incised by fluvial channels indicates aqueous activity occurred in Gale after the deposition and lithification of these materials (Malin & Edgett, 2000; Milliken et al., 2010; Pelkey & Jakosky, 2002, 2004). In contrast, the composition of the Upper formation remains largely unknown (likely because of dust cover) and it lacks the channels and canyons seen across the Lower formation, observations that are consistent with deposition by nonaqueous processes (Milliken et al., 2010; Thomson et al., 2011). The erosional unconformity between the Lower and Upper formations spans an unknown amount of time, meaning the Upper formation could be as young as Amazonian in age (Thomson et al., 2011).

In parallel to the various interpretations of sediment transport and accumulation within Gale, there are multiple hypotheses for the observed changes in mineralogy as a function of stratigraphic position. It has been proposed by Bibring et al. (2006) that different secondary/alteration minerals observed across the surface of Mars record distinct climatic conditions during different periods in martian history. In that paradigm, the "phyllosian" is roughly equivalent to the Noachian period and is marked by abundant phyllosilicate for-

mation, the "theiikian" spans much of the Hesperian period and is marked by abundant sulfate formation, and the "siderikian" spans the Amazonian period and is marked by abundant anhydrous ferric oxides. In this model, the observed variations in mineralogy are the result of global environmental changes, primarily due to the drying out of the martian surface environment. Orbital observations have shown that Gale crater contains all three of these mineral classes: phyllosilicates, sulfates, and anhydrous oxidized material, including hematite (Anderson & Bell, 2010; Fraeman et al., 2016; Milliken et al., 2010; Thomson et al., 2011; Wray, 2013). However, whether these mineral phases are authigenic, detrital, formed by surface water or by groundwater is not fully constrained, nor is their formation age relative to the depositional age of the rocks in which they are found.

The variations in strata thickness and morphology described above have been linked to mineralogical changes in a broad sense: the lower member of the Lower formation contains sulfates superposed by a zone enriched in Fe-clay minerals, spectral signatures of the middle member are dominated by sulfate with subordinate clay, the upper member is spectrally dominated by sulfate, and the Upper formation is dominated by anhydrous material with spectral signatures that are similar to reflectance spectra of martian dust (Buz et al., 2017; Fraeman et al., 2016; Milliken et al., 2010). However, whether or not the various mineralogical changes in the Lower formation conform to or cut across morphologic/albedo boundaries or stratigraphic contacts has yet to be fully evaluated. Independent mineralogical and morphological mapping to evaluate such relationships can provide insight into whether or not certain mineral signatures are consistent with primary or secondary (e.g., diagenetic) processes. In addition, many of the previously published orbital observations focused on the northwest slope of Mt. Sharp, where high-resolution CRISM data are more abundant because of preparations for Curiosity's landing. These data formed the foundation for understanding Mt. Sharp's mineralogical evolution through time, and the rover continues to test hypotheses that have arisen from these observations, but they represent a spatially limited view of Mt. Sharp. An updated and more detailed assessment of mineralogy across Mt. Sharp is warranted to understand the extent to which Curiosity's observations can be used to improve interpretations of orbital data beyond the rover traverse region.

2.2. Rover Perspectives on Mt. Sharp

Curiosity began exploring Gale Crater in August 2012 and reached what is generally agreed upon as the base of Mt. Sharp in September 2014. Detailed rover observations of the geological setting, mineralogy, chemistry, and texture led to the conclusion that Gale crater once hosted a circum-neutral pH, low salinity, alluvial-fluvial-lacustrine environment with redox gradients and available CHNOPS (carbon, hydrogen, nitrogen, oxygen, phosphorus, sulfur), the combination of which represents an ancient habitable environment on Mars (Grotzinger et al., 2014, 2015). Currently in its eighth year of exploration, Curiosity has shown that the lowermost strata of Mt. Sharp are sedimentary in origin and consist of a variety of lithologies. The dominant lithology observed thus far is interpreted to be lacustrine mudstones, with evidence for fluvial-deltaic conglomerates and sandstones as well (Grotzinger et al., 2014, 2015; Hurowitz et al., 2017; Rampe et al., 2017; Stack et al., 2016). These strata have been named the Murray formation in the stratigraphic column developed by the rover team (Grotzinger et al., 2014, 2015), and current mapping indicates the Murray fm. is equivalent to the lower member of the Lower formation described in Milliken et al. (2010).

The Murray formation includes both finely laminated distal deposits and thickly laminated proximal deposits that are sporadically intercalated with prodeltaic/fluvial cross-bedded sandstones (Grotzinger et al., 2015; Rampe et al., 2017). Individual laminations of the Murray fm. can be traced for several meters and suggest a perennial lacustrine environment, with the exception of sporadic evidence of lake lowstands/desiccation cracks in the Sutton Island member (Grotzinger et al., 2015; Rampe et al., 2017; Stein et al., 2018). Consistent with observations from orbit (Buz et al., 2017; Fraeman et al., 2016; Milliken et al., 2010; Thomson et al., 2011) and rover-based evidence of a fluvial-lacustrine environment, powder X-ray diffraction data acquired by the CheMin instrument demonstrate that the Murray fm. contains hydrated minerals, including sulfates and clay minerals (Bristow et al., 2018; Fraeman et al., 2016; Rampe et al., 2017). Indeed, clay minerals are present in all of the mudstone samples examined to date along the rover traverse path (Bristow et al., 2018; Rampe et al., 2017). Data acquired by the rover cannot be used to uniquely and unambiguously determine if the clay minerals are detrital or authigenic, but the integration of morphological, chemical,

and mineralogical observations is consistent with at least some or perhaps all of the clay minerals being authigenic, and both di- and tri-octahedral clay minerals have been observed (Bristow et al., 2015, 2018).

The sulfates identified from CheMin XRD patterns include Ca sulfates (anhydrite, bassanite, gypsum) and jarosite (Martin et al., 2017; Rampe et al., 2017; Vaniman et al., 2018). Although there is no clear evidence for Mg sulfates in the CheMin data as of yet, positive correlations between elemental Mg and S in ChemCam laser-induced breakdown spectroscopy data and alpha particle X-ray spectroscopy data suggest they may be present in select targets and stratigraphically restricted zones (Hurowitz et al., 2017; Rampe et al., 2017; Rapin et al., 2019). The Ca sulfates occur as veins, nodules, and cements, suggesting multiple episodes of early and late diagenesis rather than discrete evaporite beds (Martin et al., 2017; Nachon et al., 2017; Vaniman et al., 2014, 2018).

The mudstones of the Murray formation mudstones are unconformably overlain by eolian sandstones of the younger Stimson formation, which is primarily basaltic in composition (Banham et al., 2018). These sandstones are part of a unit that exhibits distinct morphologic attributes in orbital imagery and that can be mapped in a variety of places in Gale (e.g., akin to the "mound-skirting" unit in the map of Anderson & Bell, 2010). Previous studies have interpreted this unit as eolian in origin (Anderson & Bell, 2010; Milliken et al., 2014), and in the examples observed directly by Curiosity this has been confirmed. However, it is not clear if all examples of this unit observed from orbit represent a single contemporaneous unit or if it is all eolian in origin. Though this is clearly a widespread and important morphologic unit in Gale crater, it appears to superpose and thus postdate the Lower fm. of Mt. Sharp, and as such it and the Stimson sandstones will not be discussed further here. Instead, we focus our discussion on the strata that comprise Mt. Sharp itself, particularly the mineralogy of the Lower formation.

2.3. Remaining Questions

Now that both orbital and rover-scale data have been obtained for strata within Gale crater, it is important to integrate these perspectives in order to understand how geologic processes recorded in rocks along the rover traverse path may (or may not) extend to laterally equivalent and overlying strata in other locations in Mt. Sharp. As discussed above, orbital observations show a distinct sequence of mineral assemblages in northwestern-western Mt. Sharp, and previous unpublished results suggested similar mineral signatures may be present elsewhere in Mt. Sharp (Milliken, 2011). Though a number of additional CRISM images have been acquired since the initial study of Milliken et al. (2010), a detailed analysis of the full extent and distribution of clay minerals and sulfates throughout Mt. Sharp has not yet been published. It is also clear from rover-based observations that the stratigraphy of lowermost Mt. Sharp (and units along the rover traverse to the north) is more complex than a simple "layer cake" model, as discussed in Stack et al. (2016). This raises questions as to whether or not the large scale sulfate/clay mineral to sulfate to anhydrous oxide mineral transitions described in Milliken et al. (2010) may also be an oversimplification.

The origin and extent of the chemical and mineralogical variations that Curiosity has documented in the Murray fm. may result from a variety of processes, including diagenesis via acidic pore fluids (Rampe et al., 2017), lake level fluctuations and primary chemical precipitation in a redox-stratified lake (Hurowitz et al., 2017), multiple episodes of diagenetic fluid movement that lead to a nonuniform distribution of secondary phases such as Fe oxides, phyllosilicates, sulfates, and hydrated silica (Fraeman et al., 2016), or a combination of these processes. If many of the hydrous phases observed by the Curiosity rover are the result of postdepositional diagenetic processes, then this has important implications for interpretation of orbital data for other locations in Mt. Sharp. As an example, determining if sulfates of the middle and upper members of the Lower formation, which have yet to be observed by the rover, occur as primary evaporite deposits (e.g., discrete salt beds) or as diagenetic phases (e.g., cementing agents) is an important distinction when attempting to use the presence of such minerals as indicators of past environmental conditions. Although this cannot be fully determined from orbital data alone, mineralogical boundaries can be mapped and compared with stratigraphic, morphologic, and/or topographic boundaries. Mineralogical boundaries that clearly cut across bedding are likely to be indicative of secondary (e.g., diagenetic) processes, whereas those that conform to stratigraphic boundaries may be more indicative of primary depositional processes (with the caveat that diagenetic processes may also exhibit stratigraphic control). Similarly, if the clay minerals observed in

the mudstones along Curiosity's path are authigenic (Bristow et al., 2018), thus allowing for their formation well after the proposed phyllosian period of Bibring et al. (2006), it is important to understand how common this process might have been in Mt. Sharp as a whole by understanding the full extent of clay mineral occurrences within the Lower formation.

To address these and other questions, we have utilized new processing methods of CRISM data that allow for improved mineral identification and mapping within Gale crater, with an emphasis on the mapping of hydrous phases in lower Mt. Sharp. Mineralogical boundaries are compared with key stratigraphic transitions that were mapped using HiRISE images, including the lower-middle-upper member contacts and the marker bed of Milliken et al. (2010). In this study, we discuss the major mineralogical attributes of Mt. Sharp and the extent to which these features are present in the current and future rover traverse region. Several hypotheses that may explain the observed mineral signatures are presented, with a focus on those that can be tested by the Curiosity rover in order to better understand the extent to which observations along the traverse path can or should be scaled up to explain characteristics observed elsewhere in Mt. Sharp based on observed in orbital data.

3. Methods

3.1. CRISM Data Processing

CRISM collects hyperspectral images of the martian surface spanning the 0.3646–1.0560 and 1.0013–3.9368 μm ranges with the visible-near infrared and infrared (IR) detectors, respectively (Murchie et al., 2007). In Full Resolution Targeted (FRT) mode, the instrument is able to achieve a resolution of 18 m/pixel (Murchie et al., 2007). CRISM data can be affected by variability in spacecraft and observation conditions, including atmospheric conditions, photometric angle, surface temperature, and detector temperature (McGuire et al., 2009; Murchie et al., 2007, 2009). Such factors are especially prevalent in images of Mt. Sharp acquired in regions other than the west-northwest, leading to greater uncertainty in mineral identifications in those locations (e.g., southeastern Mt. Sharp in particular). Standard processing methods have had a difficult time adapting to these adverse effects in a way that can produce spectra high-quality enough for confident mineral detections, particularly in these images in areas other than the northwest. Therefore, although a number of CRISM images exist across Mt. Sharp, nonstandard processing methods are required to retrieve improved surface reflectance spectra. New processing techniques developed and validated by Itoh and Parente (2021) now allow for greater spectral clarity compared with methods previously used for mineral mapping in Gale crater, which in turn allows for improved confidence in mineral detections and their spatial variability across Mt. Sharp.

Spatial variations in mineralogy were assessed using 10 visible-shortwave infrared (0.4–2.5 μm) CRISM images that were processed using this new technique, which includes new atmospheric correction and de-noising methods as described in Itoh and Parente (2021). This method corrects for four major complications in CRISM data: atmospheric absorptions/distortions, severe random detector noise, interpolation bias resulting from correcting for bad pixels, as well as spectral features associated with water ice aerosols if they are observed in visual inspection (Itoh & Parente, 2021). Compared with commonly used volcano-scan correction, the method significantly reduces artifacts relevant to the absorption of CO_2 gas in the atmosphere, such as a zigzag artifact over the 1.3–1.8 μm and a bowl-shape artifact over 1.9–2.1 μm (Leask et al., 2018; Wiseman et al., 2016), while retaining surface contribution such as a water-bearing band at 1.9 μm. In addition, it also avoids spurious features (Leask et al., 2018) caused by the combination of interpolation bias and TRR3 filtering by using reprocessed I/F data without the filtering and bad pixel interpolation.

Under the assumption of approximately uniform atmosphere over an image scene, atmospheric residuals are common throughout the image column that shares a unique spectral response function for each spectral band. Thus, correcting atmospheric residuals is equivalent to correcting for column dependent artifacts. Further we assume that such artifacts are independent from surface contribution and cannot be fit with the signal model, these artifacts can be extracted and removed as a common residual of the model fitting. The method realizes this idea as an alternating optimization approach. It starts from transmission spectra in the ancillary data records distributed with the CRISM Analysis Toolbox. First the signal model is fit to all

Table 1
Compact Reconnaissance Imaging Spectrometer for Mars Images Used for Mineral Mapping

FRT00020AC4	FRT0000C518
FRT0000B6F1	FRT0001BBA1
FRT00017327	FRT000095EE
FRT00018C29	FRT00017D33
FRT00019DD9	FRT0002376B

Note. Locations of each image can also be seen in Figure 1b.

the spectra in the column by model inversion. Then, a common residual component is extracted and a transmission spectrum is updated by taking it into account. The updated transmission is then used for model fitting in the next step. Severe noise is detected between these two operations by assessing the magnitude of the residual. These operations are repeated until convergence. Robustness to different kind of noise is guaranteed by the use of an L1-error metric. Final correction is performed by removing the estimated transmission component from the I/F spectra.

The resulting corrected spectra are of sufficient quality that spectral analysis can be based on the output reflectance spectra without the need for spectral ratioing, the latter being a process where spectra from select pixels or an entire CRISM image are divided by the spectrum of a spectrally "bland" region in order to reduce noise, reduce atmospheric contributions, and enhance weak spectral features (Ehlmann et al., 2008; Milliken et al., 2010; Mustard et al., 2005, 2008). Eliminating the need for spectral ratioing reduces the risk of inadvertently removing, creating, or inverting spectral features that are not the result of noise (that is, accidentally producing false spectral characteristics). The 10 CRISM images used in this study are FRT shortwave-infrared L-cubes (1.002–3.920 μm) (Table 1, Figure 1b). Spectral analyses were based on data from 1.0–2.5 μm to avoid issues associated with thermal emission and strong atmospheric absorptions at wavelengths >2.5 μm.

Individual spectra and spectral map products derived from CRISM data processed with these new methods exhibit a reduction in noise and an increase in the spatial coherence of absorption features (mineral detections). Examples of these improvements for CRISM data of Mt. Sharp are presented in Figure 2. Previous CRISM-based mineralogical analyses across Mt. Sharp demonstrated the presence of clay minerals and sulfates in select locations, but these studies commonly relied on spectral ratio methods (Fraeman et al., 2013; Milliken et al., 2010; Thomson et al., 2011; Wray, 2013), which can be subject to error or accidentally remove spectral features of interest. Importantly, CRISM data processed with the method described above reveal clear absorption features in the output reflectance spectra (Figure 2), which (1) confirms these features are not merely artifacts and (2) demonstrates that the spectral features can be viewed in the data without relying on the spectral ratio method. Newly processed CRISM data for Gale crater provide a clearer and more reliable depiction of the spatial distribution of minerals in Mt. Sharp.

3.2. Mineral Identification and Mapping

Stratigraphic and lateral variations in mineralogy are assessed using the 10 newly processed CRISM image cubes. The processed cubes are integrated in a geographic information system (GIS) framework and georeferenced to overlapping Context Camera (CTX) and HiRISE images, which requires a slight spatial warping of the CRISM-derived products to remove offsets between the datasets due to different viewing geometries. Spectral parameter maps (e.g., band depth maps) were calculated using the methods of (Pelkey et al., 2007) and (Viviano-Beck et al., 2014) and by relying on the CRISM Analysis Toolkit made publicly available through the NASA Planetary Data System by the CRISM team. The parameters most heavily used for analysis were BD1900 (depth of the 1.9 μm H_2O absorption), BD2100 (depth of the 2.1 μm absorption related to monohydrated minerals) (Pelkey et al., 2007), and SINDEX (spectrum convexity related to hydrated sulfates) (Viviano-Beck et al., 2014). These spectral parameter maps were evaluated and used to highlight spatially coherent regions with interesting spectral features (e.g., Figure 2). Each region of interest, including regions with subtle color differences in red-green-blue composites of different parameter maps, was manually examined via the individual spectrum for that pixel as well as spectra for 5 × 5 pixel averages throughout the area of interest. The individual spectra and the bulk spectral properties of a given region of interest (ROI) were then interpreted based on absorption band positions and shapes relative to laboratory spectra from various spectral libraries (Figure 3).

In the 1.0–2.5 μm wavelength region that was used for analysis, absorptions due to the presence of OH and/or H_2O are the dominant spectral features. Reflectance spectra of most hydrous minerals exhibit absorptions with reflectance minima near ~1.4 and ~1.9 μm that arise from combination and overtone vibration

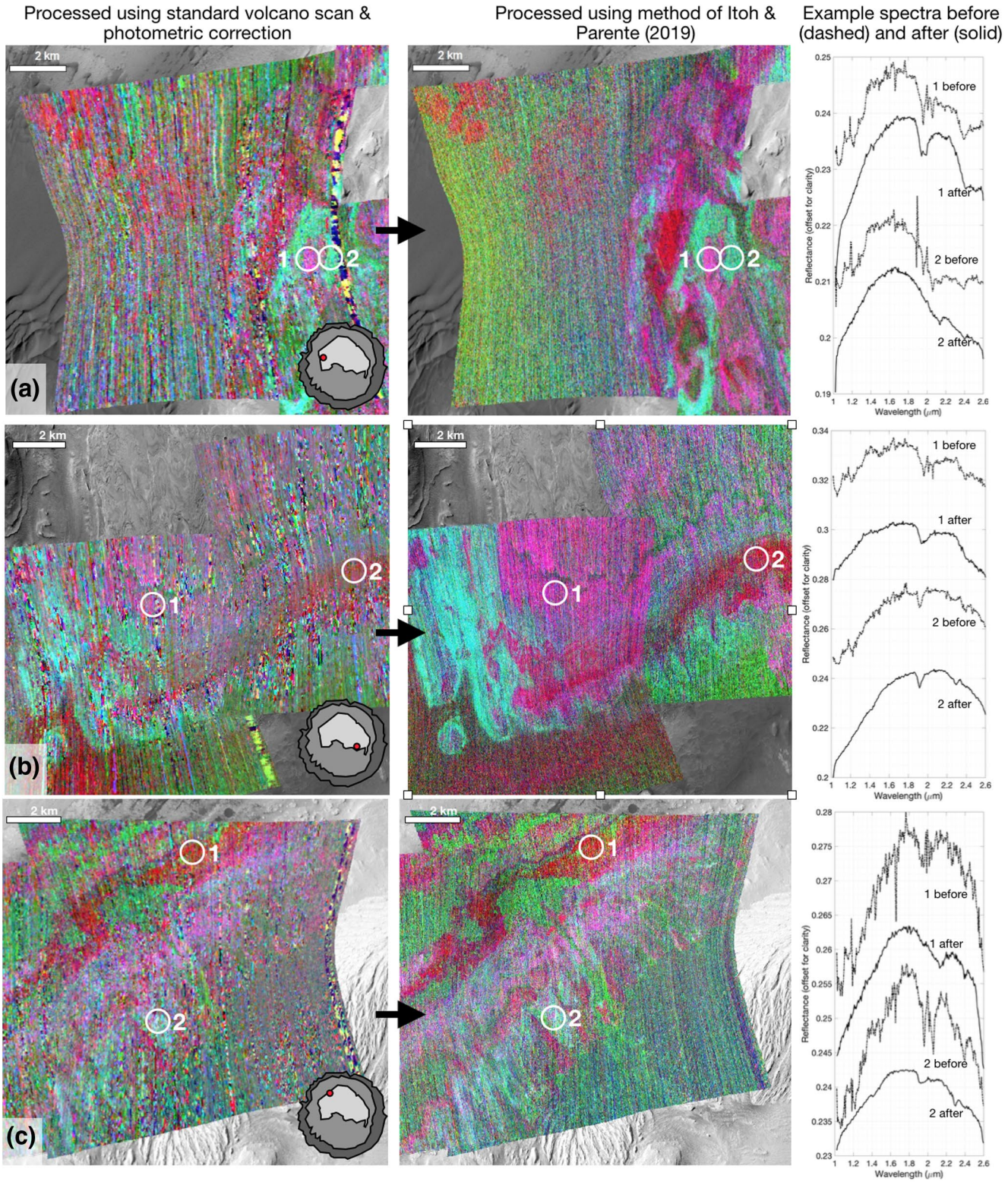

Figure 2. Comparison of spectral parameter maps (red: BD1900, green: BD2100, blue: SINDEX) created using Compact Reconnaissance Imaging Spectrometer for Mars (CRISM) Full Resolution Target images processed using standard CRISM Analysis Toolkit volcano scan and photometric correction (left column) and the method described in Itoh and Parente (2021) (middle column). For each of the locations, the red dot in the inset schematic shows the general position of the data in Gale crater. Example spectra from highlighted regions are shown in the right column. (a) CRISM image 17327, western Mt. Sharp. (b) Images 17D33 and 19DD9, southeastern Mt. Sharp. (c) Image B6F1, northwestern Mt. Sharp. Location of the central pixel (sample, line) for each spectrum, from top to bottom in each panel, are: (a) [17327] 116, 148, [17327] 78, 148. (b) [17D33] 265, 427, [19DD9] 274, 211, (c) [B6F1] 347, 416, [B6F1] 452, 92.

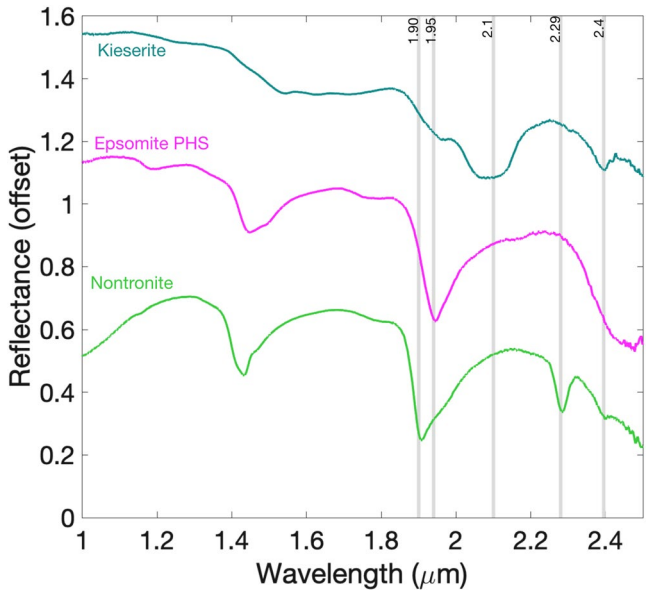

Figure 3. Laboratory reflectance spectra of kieserite ($MgSO_4 \cdot 1H_2O$), epsomite (representative of a polyhydrated Mg sulfate), and nontronite (Fe-rich dioctahedral smectite). Relevant absorptions are highlighted, for a description of absorptions used for identification in CRISM data see Table 2. PHS, polyhydrated sulfate.

modes of OH and H_2O molecules (Bishop et al., 1994; Burns, 1993; Clark et al., 1990). The spectral characteristics of OH features are influenced by the cation to which OH is attached and H_2O features are influenced by the cation and degree of hydrogen bonding to other H_2O molecules (if applicable for a given mineral). The subtleties of these features as observed in the processed CRISM data and how the features were used to interpret specific minerals or mineral assemblages are described in greater detail in the Results section. These steps and the manual verification of features observed in the spectral maps allow color variations in the spectral parameter maps that corresponded to true spectral differences to be distinguished from those caused by other factors (i.e., spectral artifacts that result in false positives in spectral parameter maps). Once a spatially coherent region with interesting spectral properties was identified using this combined parameter map and spectral examination approach, it was then mapped as a polygon using the ESRI ArcGIS software. After each of the 10 CRISM images were fully mapped, individual polygons of similar spectral type were assumed to represent similar mineral assemblages and were merged to create a final spectral unit or "mineral" map for the study region.

3.3. Mapping of Contacts and Morphological Attributes

Geomorphic-based mapping was carried out using HiRISE and CTX visible images and was conducted independently from the spectral analyses, though all data were integrated into a common GIS project. This step focused on mapping the extent of three distinct features associated with the Lower fm. of Mt. Sharp: the transition from lighter to darker-toned strata (lower-middle member contact), the transition from darker to lighter-toned strata (middle-upper member contact), and the location of the enigmatic "marker bed" (Milliken et al., 2010) (Figures 4 and 5). Tone (i.e., distinguishing between bedrock of different albedos) is used as a qualitative parameter within individual HiRISE and CTX images such that the identical stretch scale allows for direct qualitative comparison of albedo. Mapping the exposure, continuity, thickness, and boundaries of the darker-toned middle member allows us to address whether depositional or diagenetic information could be recorded in the presence of those layers, including (1) whether mineral changes co-occur with changes in outcrop tonality and morphology and (2) whether the vertical distance between these transitions or the apparent thickness of the dark band is consistent wherever it is exposed across Mt. Sharp.

The marker bed is particularly distinct in that it is bench-forming, appears smoother than adjacent units, and is lithified enough that it retains craters (Figure 5). As will be discussed below, this bed, which is particularly well-expressed in the northwest part of the mound (Milliken et al., 2010), is also observed in the southeastern part of the mound (Figure 5). As such, its position in HiRISE and CTX digital terrain models can be used as an elevation baseline to determine the relative stratigraphic heights of different mineralogical signatures identified in CRISM data.

4. Results

4.1. Key Stratigraphic Contacts in Lower Mt. Sharp

The dark-toned strata of the middle member can be mapped in a variety of locations around Mt. Sharp based on its albedo, approximate stratigraphic position, and similar geologic expression. Their occurrence is not continuous, often due to erosion and talus, but its appearance is widespread and consistent wherever it outcrops. The dark strata are consistently bounded above and below by sharp transitions into lighter-toned strata. The absolute elevation of these boundaries varies widely around Mt. Sharp. The upper boundary of the darker strata occurs at an elevation as high as ~−2,900 m in the southeast but as low as ~−4,000 m

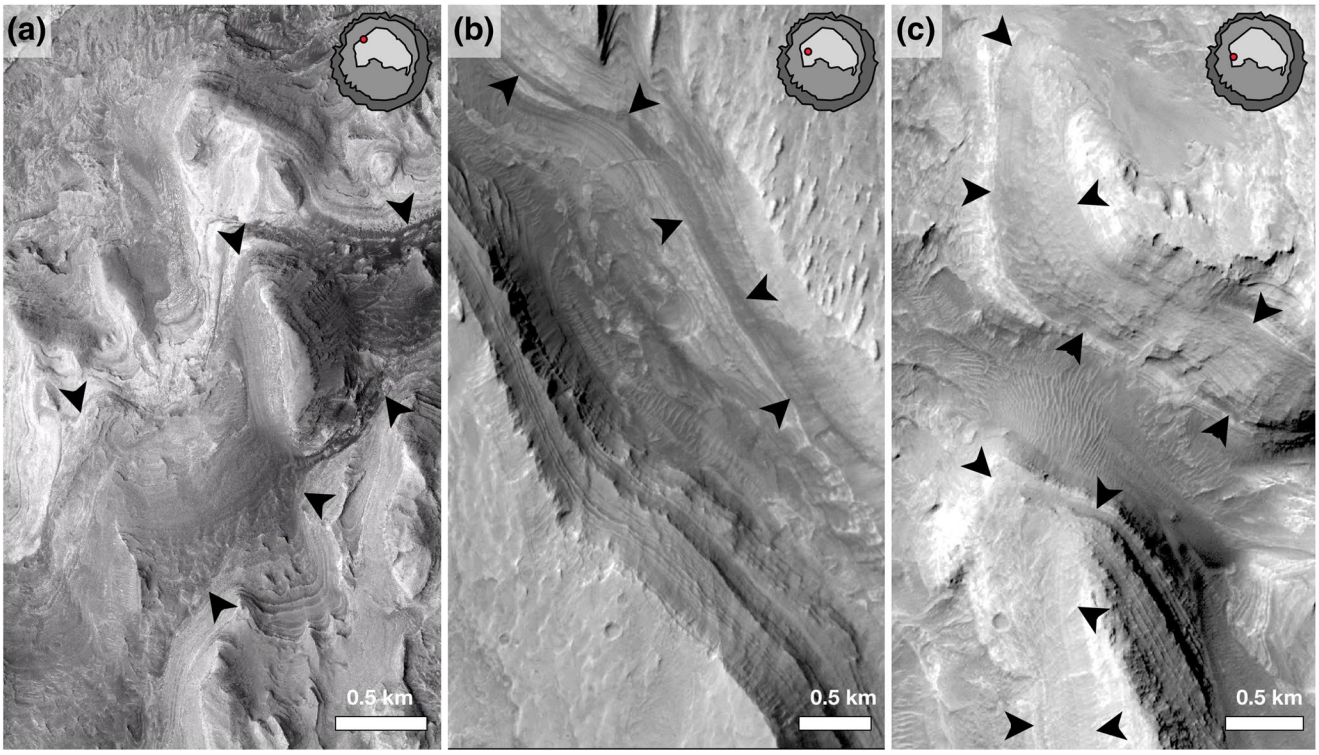

Figure 4. Examples of the light-dark-light tone transition observed around Mt. Sharp. Transitions above and below are marked with arrows. (a) Exposure on northwestern Mt. Sharp. (b) Transition exposed on the eastern face of the "grand canyon" in western Mt. Sharp. (c) Transition exposed on either side of a large canyon in southwestern Mt. sharp.

elevation in the northwest (Figure 6). Given the widespread exposure of the dark-toned strata and their widespread exposure throughout Mt. Sharp, it is worth constraining the thickness of this package of strata and assessing variations in apparent thickness. Using the position of the marker bed as a "datum," and by measuring the distance from the marker bed to the top and bottom of the darker-toned strata, we find that the dark-toned zone varies significantly in apparent thickness across Mt. Sharp (Figure 6). The apparent thickness, which does not correct for the dip angle of the beds, is calculated by the change in elevation between the lower and upper boundaries of the dark-toned zone. Using this approach, the thinnest exposure is measured to be 38 m and the thickest is measured to be 255 m. Although the exact bedding geometry of strata within the middle member is not known at all locations, previous measurements of the dip values across lower Mt. Sharp generally indicate relatively small values of 1°–4° northwest (Kite et al., 2013; Milliken et al., 2010), although recent work also finds dip values of up to 28°, sometimes northwest and sometimes southwest (Anderson et al., 2018). Given these small variations in dip angle, it is extremely unlikely that differences in bedding geometry alone can account for such a wide range in apparent thickness (~38–255 m). This suggests that the true stratigraphic thickness of the dark-toned strata of the middle member is highly variable across Mt. Sharp.

It is also clear in HiRISE and CTX images that there are additional dark bands or strata in Mt. Sharp that occur below the more coherent package of strata in the middle member. These additional dark bands can be seen in Figures 4a and 4c; they are not particularly erosionally resistant like the marker bed but they do appear to be relatively thin.

We also observed that the marker bed occurs within a thick zone of lighter-toned strata rather than as a potential capping unit to the darker-toned strata of the middle member as previously depicted in Milliken et al. (2010). The previous stratigraphic column of Milliken et al. (2010) relied heavily on the attributes of the NW portion of Mt. Sharp, where the marker bed is indeed stratigraphically close to the upper limit of the dark-toned strata of the middle member (e.g., see bottom left corner of Figure 10a). However, where the

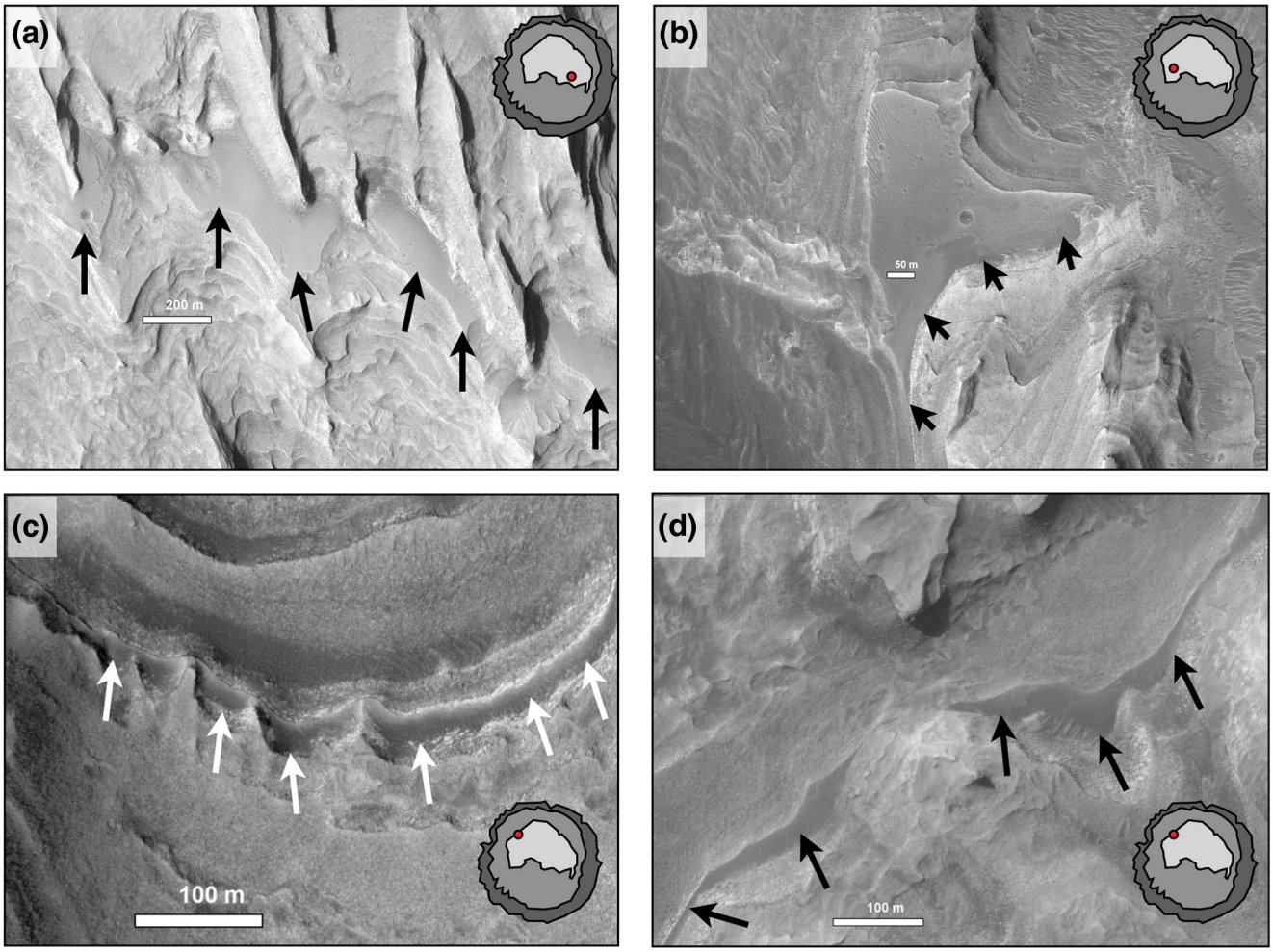

Figure 5. Examples of exposures of the dark, smooth, crater retaining "marker bed" around Mt. Sharp. The position is indicated by the red dot in the crater schematic inset at the top right of each panel. (a) Southeast Mt. Sharp, exhibiting craters. (b) Southwest Mt. Sharp, exhibiting craters. (c) Northwest Mt. Sharp. (d) Northwest Mt. Sharp.

marker bed is observed in other locations in Mt. Sharp it is clear that it also occurs stratigraphically above the upper boundary of the darker-toned strata, at least in a relative sense. Therefore, if the marker bed is used to define the boundary between the middle and upper members of the Lower formation, then the middle member encompasses both the coherent package of darker-toned strata described above as well as overlying lighter-toned strata.

Like the darker-toned strata, the marker bed is found to occur at a range of absolute elevations, from around −3,800 m in the northwest to around −2,600 m in the southeast; the apparent elevation change (i.e., stratigraphic thickness) between the top boundary of the dark-toned strata to the marker bed is also enormously variable (Figure 6). Although it is traceable for many tens of kilometers, the marker bed is not as laterally continuous as the band of darker-toned strata. Because of this, it is possible that the apparent variation in the elevation of the marker bed could actually be due to outcropping of multiple "marker" beds at different elevations.

4.2. Mineralogy

Based on the analysis of the newly processed CRISM images, we find that the mineralogy of Mt. Sharp can be divided into six major spectral classes and mixtures thereof: monohydrated (likely Mg-) sulfate,

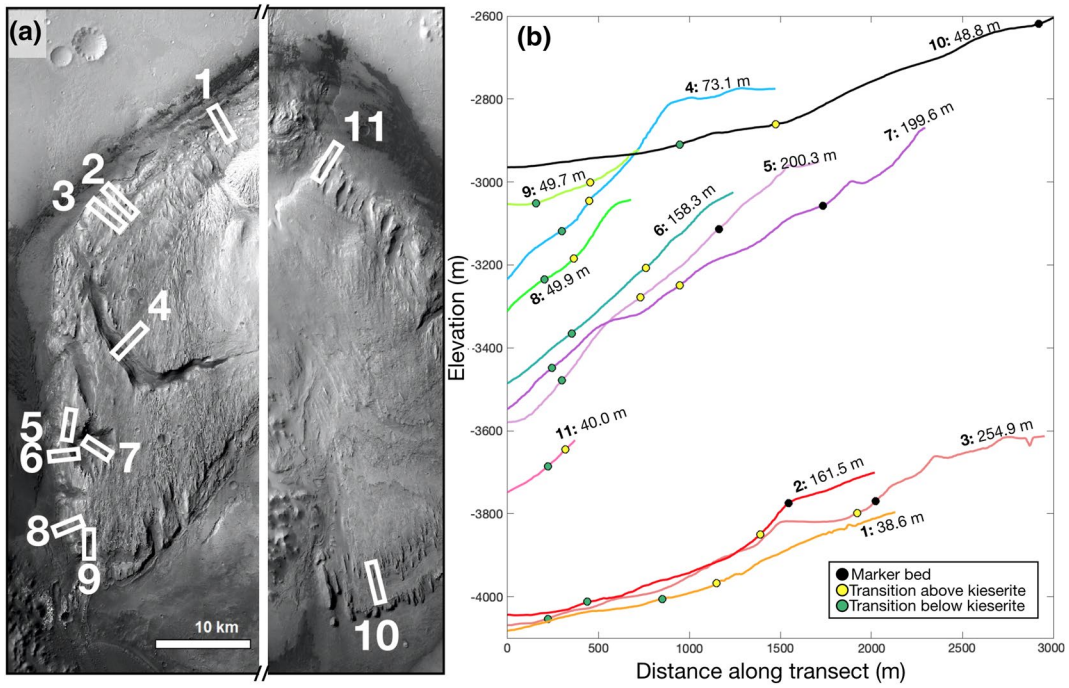

Figure 6. Sample elevation profiles from various locations around lower Mt. Sharp. (a) White rectangles on a Context Camera (CTX) mosaic mark the locations of 11 places where the dark-toned strata are exposed. (b) Elevation profiles of the 11 transects in (a), based on CTX digital terrain models with 6 m postings; for each profile, the yellow dot marks the contact of the top of the dark-toned strata, the green dot marks the bottom of the dark-toned strata, and the black dot denote the position of the marker bed, when visible. Each profile is labeled with the vertical distance (in meters) between the upper (yellow) and lower (green) contacts, that is, the apparent thickness of the darker kieserite-bearing band.

polyhydrated (likely Mg-) sulfates, phyllosilicates, mafic minerals (olivine/pyroxene), spectrally bland materials, and undifferentiated hydrous materials, as well as mixtures thereof. Their presence is broadly consistent with the results of previous studies (Buz et al., 2017; Fraeman et al., 2016; Milliken et al., 2010; Rampe et al., 2017), though the methods used in this study allow for increased confidence in these detections, particularly for CRISM images acquired with elevated detector temperatures or during nonideal atmospheric conditions. It should be highlighted that spectral features for Fe oxides, which are visible in CRISM data as reported by Milliken et al. (2010) and Fraeman et al. (2013), are found at shorter wavelengths than in the L-data used in this study, which is why Fe oxides are not a spectral class identified here. The spectral characteristics used to map pixels into these classes are described in detail below and summarized in Table 2. Examples of each spectral class, including spectral mixtures, are presented in Figure 7.

4.2.1. Monohydrated Sulfate

Pixels whose spectra exhibit a strong 2.1 μm absorption, often somewhat boxy in shape and starting near ~1.9 μm, in conjunction with a weaker but sharp 2.4 μm absorption, are characterized as monohydrated sulfate. The 1.9–2.1 μm feature is caused by H_2O interacting with the sulfate ion (Gendrin et al., 2005), whereas the 2.4 μm feature is caused by $(SO_4)^{2-}$ stretching vibrations (Cloutis et al., 2006). There is a notable lack of a 2.3 μm feature in these spectra, meaning the 2.4 μm feature cannot be attributed to an overtone feature in clay minerals. Kieserite ($MgSO_4$ H_2O) is the best spectral match for these features (Cloutis et al., 2006; Mangold et al., 2008), as spectra of monohydrated Fe sulfate (e.g., szomolnokite) exhibit a broad Fe^{2+} band from 1.2 to 1.6 μm that is not observed in the CRISM data as well as a slightly different shape to the 2.1 μm feature (Mangold et al., 2008).

4.2.2. Polyhydrated Sulfate

Pixels whose spectra exhibit a strong 1.93–1.95 μm absorption and a strong drop in reflectance after ~2.3 μm are characterized as polyhydrated sulfate (PHS). The drop in reflectance is due to the strength of broad 2.4 μm absorption (Clark et al., 1990; Cloutis et al., 2006; Gendrin et al., 2005; Mangold et al., 2008). In particular, epsomite ($MgSO_4 \cdot 7H_2O$) or hexahydrite ($MgSO_4 \cdot 6H_2O$) are good spectral fits, but we consider polyhydrated Mg sulfates (hereafter PHS) as a group, not distinguishing the particular form of sulfate or number of water molecules (n) other than $nH_2O \geq 1$.

We note that this spectral class excludes Ca sulfates such as gypsum ($CaSO_4 \cdot 2H_2O$) or bassanite, whose spectral features are diagnostic and include a triple absorption near 1.4 μm, a weak absorption band at 1.75 μm, and a doublet absorption with local minima at 2.21–2.27 μm (Cloutis et al., 2006; Mangold et al., 2008). None of these features are apparent in the CRISM data examined in this study, thus the cation associated with the PHS spectral class is unlikely to be Ca^{2+}. Spectral studies of other areas of Mars have also concluded that Mg sulfates are the best match for the types of features observed in our data (Bishop et al., 2009; Gendrin et al., 2005; Mangold et al., 2008; Roach et al., 2010), though we cannot fully exclude other cations or mixed-cation species (e.g., Mg-Na sulfates).

4.2.3. Phyllosilicates

CRISM spectra that exhibit a strong 1.9 μm absorption and a weaker but distinct narrow 2.2–2.3 μm absorption were characterized as phyllosilicates, that is, clay minerals. The 2.2–2.3 μm absorptions are caused by combination bend and stretch metal-OH vibrations, with the band center depending on the octahedral cation to which the OH is attached. Specifically, this absorption will exhibit a reflectance minimum at ~2.28 μm for Fe-OH (e.g., the smectite nontronite), ~2.2 μm for Al-OH (e.g., montmorillonite and kaolinite), and ~2.31 μm for Mg-OH (e.g., the smectite saponite) (Bishop et al., 2008; Clark et al., 1990). Weak absorptions at ~1.4 and ~2.4 μm were also observed in spectra of ROIs where the clay mineral signal was especially strong, but the presence of these absorptions were not required for classification as phyllosilicate-bearing. Where observed in CRISM data of Mt. Sharp, the metal-OH absorption commonly exhibits a reflectance minimum at 2.29 μm (Figures 7a and 14d, 14e and 14g), a position that is most consistent with Fe-smectite (e.g., nontronite) possibly with minor Mg^{2+} substitution (Michalski et al., 2015). Many of the CRISM phyllosilicate spectra also exhibit a weaker absorption on the shorter wavelength side of the primary metal-OH band, and this shoulder is consistent with the presence of Al^{3+} substituted into the octahedral layer or a separate Al-rich clay mineral (Milliken et al., 2010). It is worth noting that in a few locations the metal-OH absorption is shifted to slightly longer wavelengths (Figure 8) that could indicate increased Mg^{2+} content, consistent with either Mg-smectite or possibly a mixed layer chlorite-smectite. Reflectance spectra of mixed-layer chlorite/smectite (e.g., corrensite) tend to exhibit an asymmetrical absorption with a minimum near ~2.31–2.33 and a very weak 2.4 μm absorption (Milliken & Bish, 2010). Clay mineral identifications with this band position are almost exclusively found in the crater floor in areas that are classified as spectrally mixed clay mineral/mafic (Figure 8, spectra 1–3). One potential detection is found within Mt. Sharp in the southwest, at a high stratigraphic position in CRISM image FRT00018C29 (Figure 8, spectrum 4).

4.2.4. Mafic

Spectra that exhibit broad absorptions with reflectance minima near ~2 and/or ~1 μm were classified as mafic and are interpreted as olvine, pyroxene, or mixtures of these phases. These absorptions are the result of crystal field splitting due to Fe^{2+} in octahedral coordination (Burns, 1993), and they are commonly observed in low albedo regions on Mars (Bibring et al., 2006; Murchie et al., 2009; Mustard et al., 2005; Poulet et al., 2009). In pyroxene minerals, the center of these absorptions shift to longer wavelengths as Ca content increases, meaning that spectra of orthopyroxenes exhibit absorptions centered near ~0.9 and ~1.8 μm whereas spectra of clinopyroxenes (augite) exhibit absorptions near ~1.05 and 2.3 μm (Adams, 1974; Cloutis & Gaffey, 1991; Klima et al., 2011; Sunshine et al., 1993). The center of the ~2 μm pyroxene absorption observed throughout Mt. Sharp and deposits around its base is commonly at ~2.08 μm (Figure 7), consistent with a pyroxene of intermediate Ca content.

Table 2
Spectral Characteristics Used for Mineral Identification

Ascribed mineralogy	Spectral features
Monohydrated sulfate (e.g., kieserite)	Strong 2.1 (often starting ~1.9 μm), 2.4 μm
Polyhydrated Mg sulfate	1.93–1.95 μm, drop in reflectance after ~2.3 μm
Fe-Mg clay mineral	1.90, 2.3 μm, possibly weak 2.4 μm
Mafic (olivine and pyroxene)	Broad absorptions that center at 1 and 2 μm
Spectrally bland	Rounded shape with a maximum ~1.7 μm, no discernible absorptions
Undifferentiated hydrous	Nonunique water-related absorptions at 1.4, 1.9 μm
Mix: Kieserite & PHS	1.93–1.95 possibly extending out into a weak 2.1, 2.4 μm
Mix: Clay mineral & PHS	1.90–1.93, 2.28–2.3, possible weak 2.4 μm
Mix: Clay mineral & mafic	1.90 and 2.3 μm absorptions superposed over a broad pyroxene absorption centered at ~2.1 μm

Abbreviation: PHS, polyhydrated sulfate.

4.2.5. Spectrally Mixed

ROIs whose spectra exhibit several of the above criteria were mapped as mixtures of these spectral classes. The methods used for mineral identification in this study are qualitative rather than quantitative, thus we do not attempt to determine relative proportions of different spectral (mineral) classes. In the mineral maps we present, regions that are spectrally mixed (e.g., clay minerals and mafics) are denoted by stripes of the two relevant colors.

4.2.6. Undifferentiated Hydrous

Some regions of interest are characterized by spectra that only exhibit nonunique H_2O-related absorptions at 1.9 μm, and in some cases 1.4 μm as well. These features indicate that at least one hydrated phase is present, but no other diagnostic absorptions are observed that could be used to uniquely identify specific minerals. In some cases, these spectral features appear rather noisy or exhibit band shapes that are broader than expected for typical H_2O-bearing minerals. Though these areas are spatially coherent, they may be due to or influenced by artifacts in the data processing procedure (e.g., incomplete or improper atmospheric corrections). Therefore, caution is warranted when interpreting the significance of the occurrences of this spectral class, but at least some fraction of CRISM spectra in each of the occurrences exhibit a distinct 1.9 μm H_2O feature.

4.2.7. Spectrally Bland

Pixels whose corresponding spectra lacked distinctive absorptions, in many cases appearing spectrally similar to the ubiquitous martian dust, were classified as spectrally bland. These spectra commonly exhibit a slight convex shape with a reflectance maximum ~1.6–2.0 μm, but they otherwise lack discernible spectral features strong and clear enough to use for identification.

4.3. Spatial Context of Mineralogical Units

Analysis of the processed spectral parameter maps (Figure 9a.) and their constituent individual spectra allows each image to be divided into the relevant spectral classes described above. The mineral distribution can then be compared with the independently mapped contacts and geomorphic features (Figure 10). The mineral maps produced by the CRISM analysis and spectral mapping are presented in Figure 9b and in greater detail in Figure 10. These maps reveal interesting details in the spatial distribution of hydrous minerals throughout Mt. Sharp when compared with key stratigraphic contacts, and in this section we summarize several of the major trends in mineralogy and how they relate to these contacts and other morphological traits.

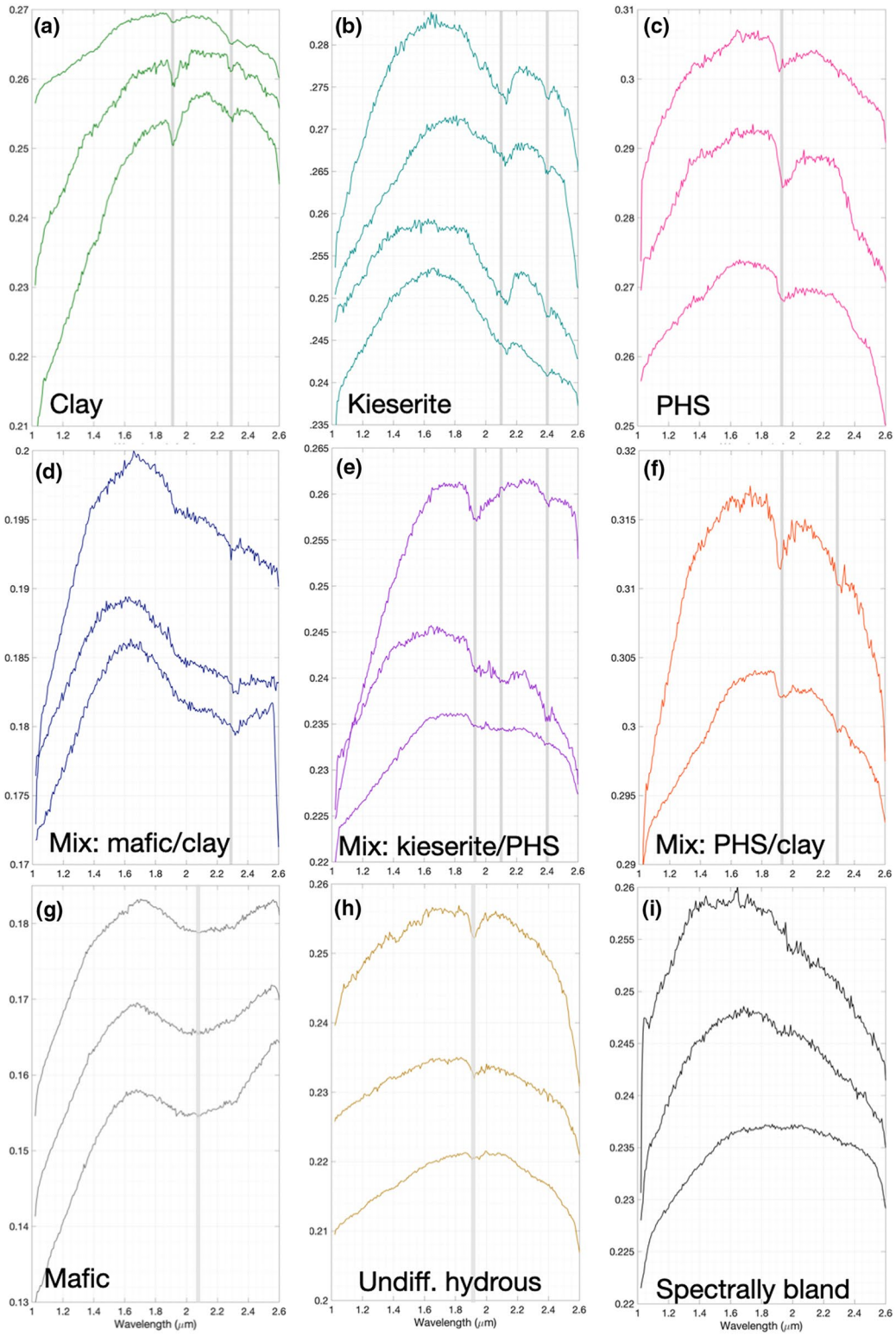
(a)
Clay
(b)
Kieserite
(c)
PHS
(d)
Mix: mafic/clay
(e)
Mix: kieserite/PHS
(f)
Mix: PHS/clay
(g)
Mafic
(h)
Undiff. hydrous
(i)
Spectrally bland
Wavelength (μm)

These results can be used to compare detailed mineral stratigraphies in different areas of Mt. Sharp (Figure 11). These columns are agnostic to whether the spectral signatures are due to talus or bedrock, which is difficult to discern from orbit. Many of the erosionally resistant hills are enriched in PHS, although some in the southeast are enriched in clay minerals.

4.3.1. Sulfate Spectral Classes

We observe that monohydrated Mg sulfate (spectrally consistent with kieserite) most commonly occurs in the middle section of lower Mt. Sharp, corresponding with the middle member of the Lower formation. Kieserite spectral features are commonly associated with darker-toned strata, but some of the strongest spectral signatures are in areas where eroded material has accumulated, particularly in valleys and other topographic lows on the southeast side of Mt. Sharp (CRISM image 17D33). That is, the strongest kieserite signatures are associated with what appear to be unconsolidated or poorly lithified deposits. Of particular note is that bedrock exhibiting kieserite signatures appears to be somewhat stratigraphically restricted. As shown in Figure 10, the darker band of strata in the middle member that is mappable in a variety of locations around Mt. Sharp (as discussed above) is enriched in kieserite everywhere it is observed. In contrast, the lighter-toned units immediately above and below these darker strata are enriched in PHS and, in some locations, CRISM spectra indicate the presence of Fe/Mg clay minerals. The boundaries between the darker kieserite and the lighter PHS/clay mineral zones appear relatively sharp at the orbital scale, and they are easily visible except in some locations where talus has accumulated on low slopes (e.g., CRISM image 17D33). Though kieserite signatures are not solely confined to the darker-toned strata of the middle member, spectra for this portion of the stratigraphic section appear to be particularly dominated by kieserite compared with other portions of lower Mt. Sharp.

PHS spectral signatures are found to occur over a wider range of stratigraphic heights compared with the kieserite detections. PHS is associated with strata/deposits that are clearly below, within or intercalated with, and stratigraphically above the kieserite-enriched zone. The strongest PHS signatures appear to be associated with intact bedrock (not unconsolidated materials). Spectrally mixed kieserite/PHS areas are not common but are found to occur in two locations that exhibit relatively shallow surface slopes, one of which is on the southeast portion of Mt. Sharp and the other is near the future rover traverse route (CRISM image B6F1). When considered as a whole, the CRISM data examined in this study indicate the spectrally dominant hydrated phase(s) of the middle and upper members, as well as some of the lower member, is PHS. The dark-toned kieserite-bearing portions of the middle member exist within a thick sequence of predominantly PHS-bearing strata.

As mentioned above, there are a number of darker bands or strata that occur below the primary darker-toned kieserite band. Though visible in HiRISE images, the lower spatial resolution of CRISM data does not make it possible to clearly determine the composition of these strata. One location where these stratigraphically lower dark bands may be resolvable in the near-IR reflectance data is on the southeast face of Mt. Sharp (Figure 12). Here, an alternating pattern of light and dark bands are observed and the corresponding CRISM data exhibit clearly different spectral signatures. In this location, spectra of the darker bands are similar to kieserite whereas the lighter bands are more spectrally similar to PHS. Neither the lighter PHS nor darker kieserite layers exhibit a clear correlation with steeper surface slopes, though such relationships have been observed in other areas on Mars where interbedded monohydrated and polyhydrated sulfate layers are present (Mangold et al., 2008; Roach et al., 2010).

4.3.2. Clay Mineral Spectral Classes

Spectral signatures of clay minerals are found to occur at a variety of elevations/stratigraphic positions in Mt. Sharp, and the strata or deposits that host these clay minerals exhibit a range of morphological attrib-

Figure 7. Example spectra for each mineral classification group. All spectra are unratioed 5 × 5 pixel (spectral) averages. Relevant absorption bands used for identification are highlighted with gray lines. (a) Clay minerals, (b) monohydrated Mg sulfate/kieserite, (c) polyhydrated Mg sulfate (PHS), (d) mix of mafic and clay minerals, (e) mix of kieserite and PHS, (f) mix of PHS and clay minerals, (g) mafic phases (i.e., olivine/pyroxene), (h) undifferentiated hydrous, (i) spectrally bland. Location of the central pixel (sample, line) for each spectrum, from top to bottom in each panel: (a) [B6F1] 568, 334, [17D33] 177, 204, [18C29] 315, 111, (b) [18C29] 287, 414, [1BBA1] 424, 88, [17D33] 421, 358, [17327] 78, 148, (c) [1BBA1] 478, 172, [18C29] 51, 423, [17D33] 265, 427, (d) [17327] 468, 276, [17D33] 184, 42, [17327] 463, 301, (e) [17D33] 299, 249, [18C29] 121, 332, [B6F1] 286, 371, (f) [18C29] 189, 427, [B6F1] 377, 383, (g) [17D33] 582, 23, [18C29] 596, 169, [17327] 588, 259, (h) [1BBA1] 286, 430, [20AC4] 291, 232, [B6F1] 591, 439, (i) [17D33] 218, 397, [18C29] 62, 72, [B6F1] 243, 231.

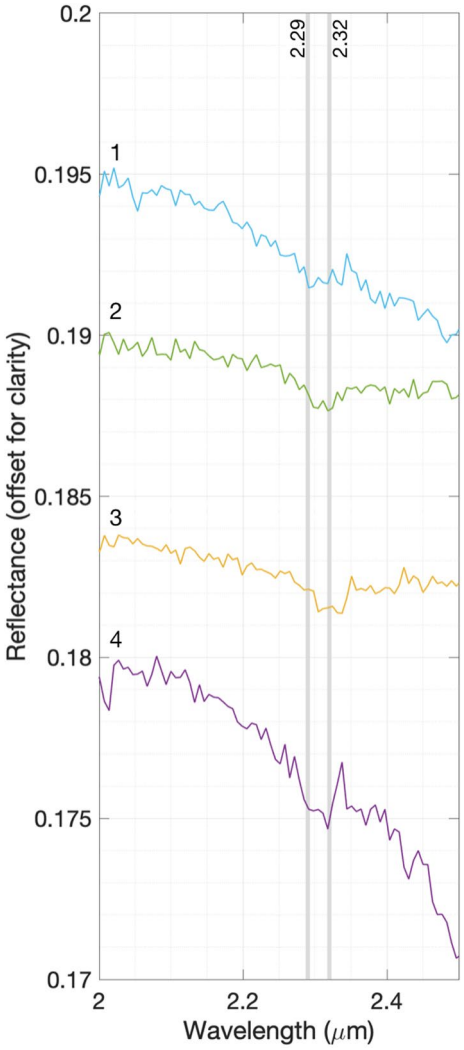

Figure 8. Examples of a potential subtle shift in metal-OH band position found in several locations in Mt. Sharp. The metal-OH absorption is commonly found to have a maximum near a wavelength of 2.9 μm, but in some locations it is slightly shifted to 2.30–2.32 μm. Location of the central pixel (sample, line) for each spectrum, from top to bottom in each panel, from top to bottom: [17D33] 184, 46; [17D33] 535, 9; [17327] 468, 276; [18C29] 189, 427.

utes in corresponding HiRISE and CTX images. The best-known example of clay-bearing materials in Gale crater is the region found in the lower member of the NW portion of Mt. Sharp (Milliken et al., 2010; Thomson et al., 2011) that lies along Curiosity's traverse path. This clay-bearing zone resides within a region referred to as Glen Torridon by the rover team and it is actively being explored by Curiosity (Figure 14d), which has confirmed with CheMin XRD measurements that it is indeed enriched in Fe-clay minerals (Bristow et al., 2019). This clay-bearing region is also known to host interesting ridge-like features that are reminiscent of bedforms or period bedrock ridges (Anderson & Bell, 2010; Bandfield et al., 2013; Milliken et al., 2014; Stack et al., 2019), and it is somewhat darker-toned than surrounding units. In addition to this "clay-bearing" region, we observe that there are other occurrences of clay minerals outside of the Glen Torridon region that exhibit similarly strong spectral features and that correspond to materials/strata with different morphologic attributes at different elevations.

From a stratigraphic point of view, there are several occurrences of clay-bearing strata that occur within the lower member and thus below the kieserite-enriched zone of the middle member (e.g., Figures 14d, 14e and 14g). However, these clay mineral occurrences cannot be traced continuously across the mound and their textural expressions vary in visible images. As an example, the morphology of this zone varies from that of the dark-toned gently sloping clay-bearing unit of Glen Torridon in northwestern Mt. Sharp (Figure 14d) to lighter-toned erosionally resistant clay-bearing strata in southeastern Mt. Sharp (Figure 14e). The latter example is particularly intriguing because it is not clear whether or not it is part of or if it superposes strata of the lower member. Clay minerals are also found to occur in locations that are clearly stratigraphically higher than the kieserite zone of the middle member. These examples of clay minerals are spectrally "pure" in some locations (Figures 13b and 13f) and mixed with PHS in others (Figure 14c). As with the clay minerals in the lower member, these occurrences are not laterally traceable across all of Mt. Sharp. Finally, clay minerals are also found to occur stratigraphically below Glen Torridon in northwestern Mt. Sharp (Figure 13a), as well as in exposures in the crater floor, where it is spectrally mixed with pyroxene (Figures 13b and 13c and 14f). The former examples, though not in the Glen Torridon region, are part of the Murray fm. and are laterally equivalent to strata encountered by Curiosity. The stratigraphic position of clay minerals exposed in the crater floor to the west of Mt. Sharp is unclear (Milliken et al., 2014), and they may represent erosional windows into strata that predate the formation of what is currently Mt. Sharp or clay-bearing units that onlap and thus postdate the formation and major erosion of the mountain.

Milliken et al. (2010) observed that portions of NW Mt. Sharp exhibited evidence for spectral mixing of clay minerals and sulfates (PHS); we confirm that finding and also observe that similar clay-sulfate mixtures and/or lateral variations in clay minerals are present in several relatively expansive areas elsewhere in Mt. Sharp. In some locations, PHS and clay minerals are spectrally mixed at the spatial scale of CRISM pixels (~18 m/pixel). This can be seen in the northwest of Mt. Sharp (B6F1 and C518, Figure 10a), where a zone that lies between distinctly clay mineral and distinctly PHS units exhibits spectrally mixed clay mineral/PHS features. In other locations, the clay mineral and sulfate signatures transition laterally into each other without strong spectral mixing. This can be seen slightly to the west of but at approximately the same stratigraphic position as the spectrally mixed band in B6F1/C518: in 1BBA1, the clay mineral and PHS areas are not mixed, transitioning between each other along relatively distinct boundaries. It is unclear at this

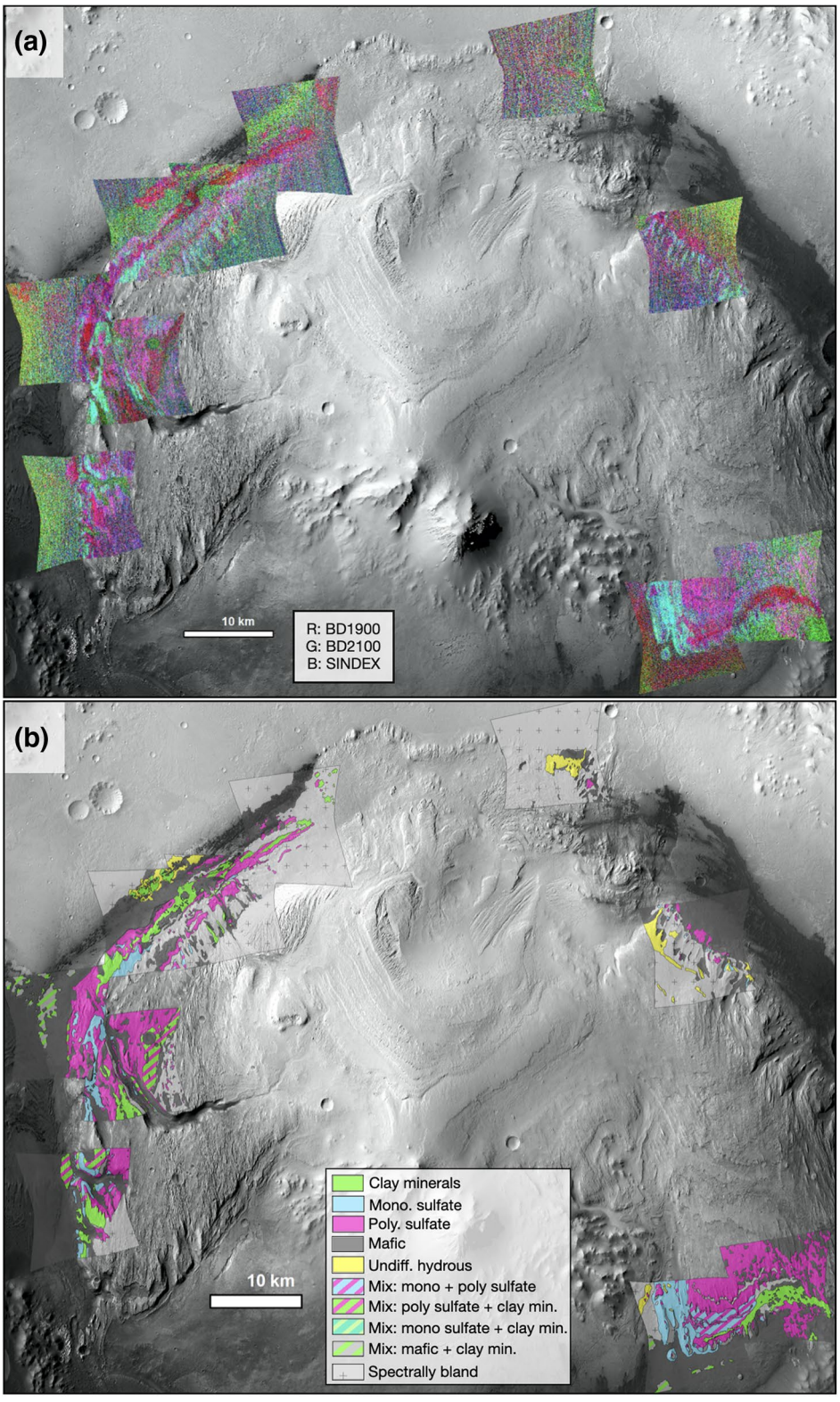

Figure 9. (a) Spectral parameter maps of the 10 processed Compact Reconnaissance Imaging Spectrometer for Mars (CRISM) images. Red channel: BD1900 (sensitive to H_2O-bearing minerals), green channel: BD2100 (sensitive to monohydrated sulfate/kieserite), blue channel: SINDEX (sensitive to hydrated sulfates). (b) Integrated mineral map of Mt. Sharp based on CRISM analysis; striped areas are spectrally mixed.

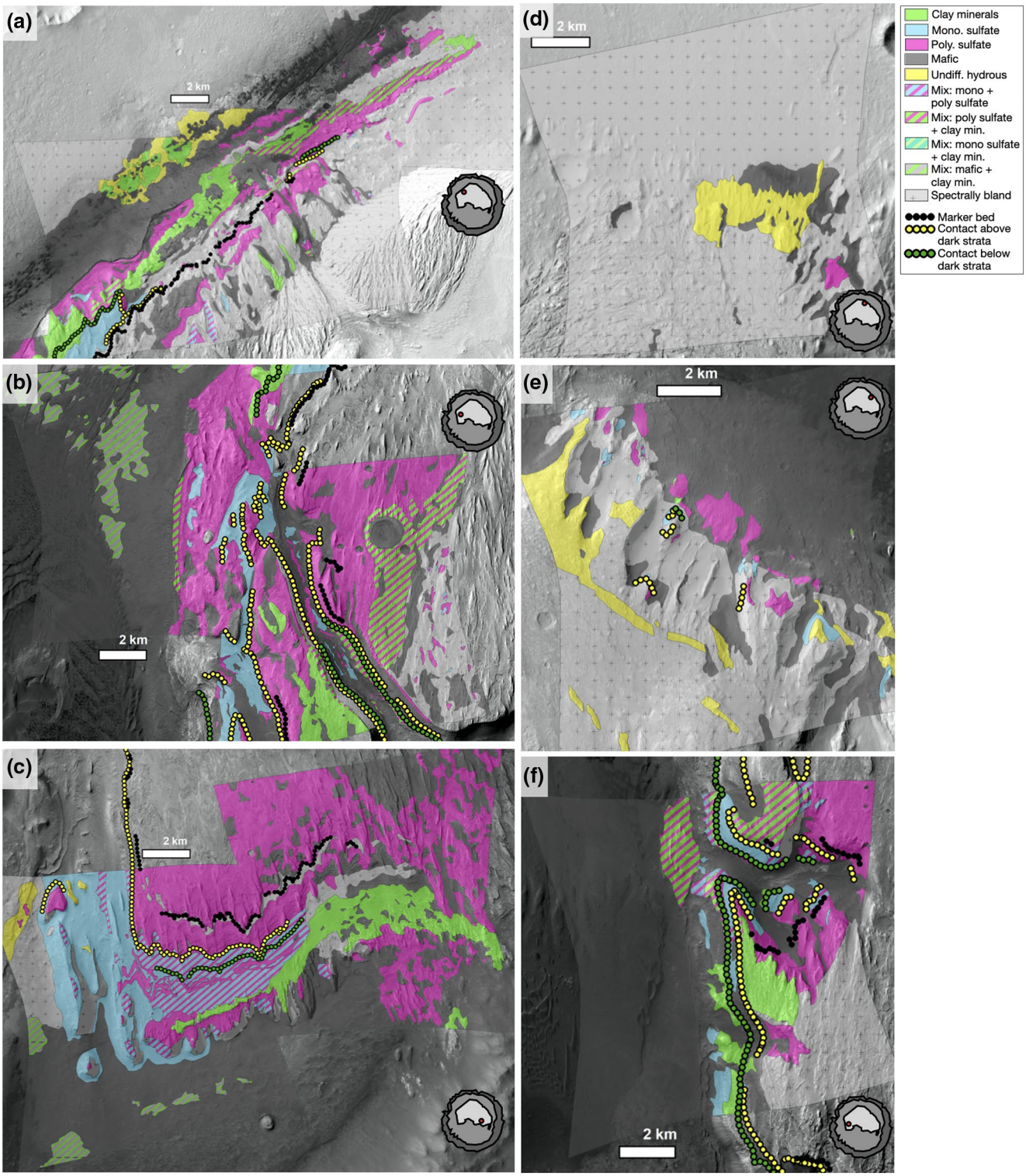

Figure 10. Zoomed-in views of the Compact Reconnaissance Imaging Spectrometer for Mars-based mineral map presented in Figure 9. Dotted line traces the contact above the dark-toned layer, bold solid line traces the contact below the darker-toned layer, and solid line traces the marker bed. (a) 1BBA1, B6F1, and C518, (b) 17327 and 95EE, (c) 17D33 and 19DD9, (d) 20AC4, (e) 2376B, (f) 18C29.

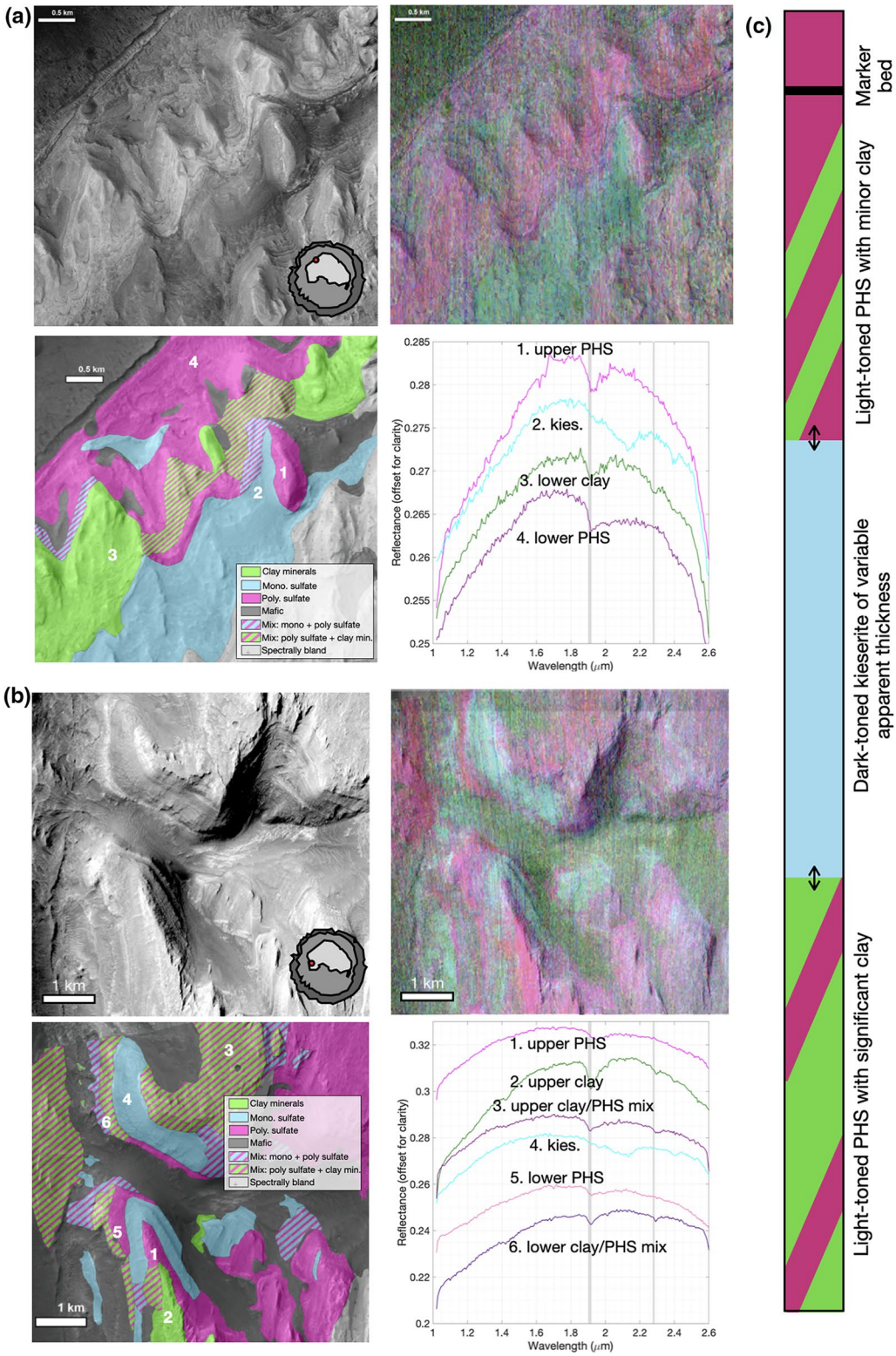

spatial resolution whether the spectrally mixed regions are the result of talus and mass wasting or actual representations of variations in bedrock mineralogy.

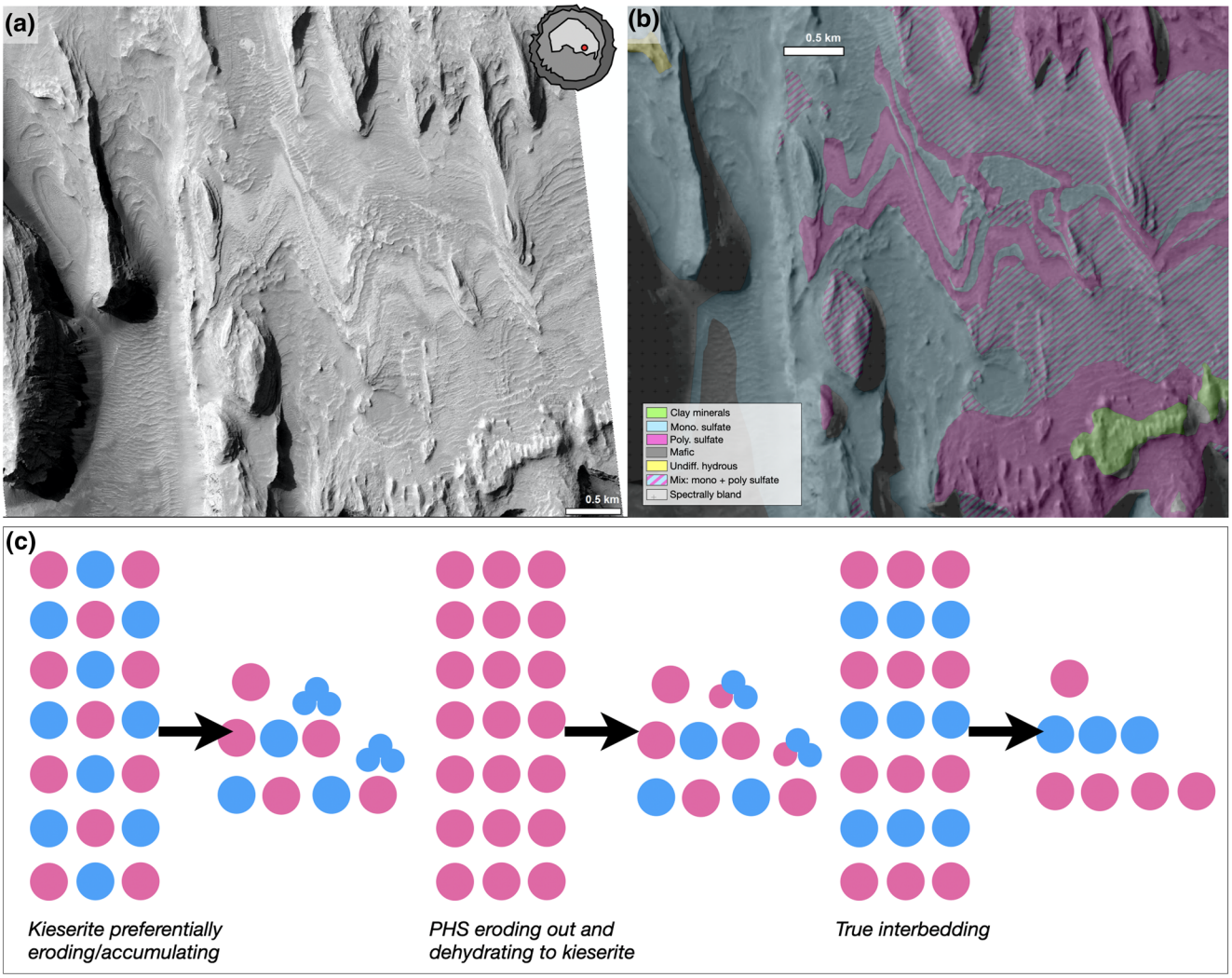

Figure 12. Vertical alternation between lighter-toned PHS-rich zones and darker-toned kieserite-rich zones observed on the southeast face of Mt. Sharp. (a) Tonality observed in HiRISE images and (b) mapped mineralogy overlain on the HiRISE images. These different mineral "bands" appear to be stratigraphically below the prominent dark kieserite band observed throughout lower Mt. Sharp. Note that the gray areas are mapped as spectrally bland, likely because they correspond to shadowed regions with low signal. (c) Schematic of possible processes that may explain the observed alternating pattern of sulfates. The first is that kieserite and PHS are truly intermixed in the strata and the kieserite is preferentially eroding out and/or accumulating on lower topographic slopes. The second is that the underlying bedrock is PHS-bearing and grains dehydrate to form kieserite as they erode out and accumulate on topographic lows. The third is that the bedrock consists of truly interbedded PHS and kieserite and that the observed spectral signatures accurately depict the hydration state of the underlying bedrock. Distinguishing between these three scenarios requires detailed in situ observations and may be possible if similar alternating patterns are observed in northwest Mt. Sharp by Curiosity. HiRISE, High Resolution Imaging Science Experiment; PHS, polyhydrated sulfate.

4.3.3. Mafic, Spectrally Bland, and Undifferentiated Hydrous Spectral Classes

Mafic spectral signatures dominate large areas of the topographically lower crater floor as well as some local topographic lows on Mt. Sharp, and these signatures are most often associated with unconsolidated materials (e.g., sand dunes or other eolian deposits) (Anderson & Bell, 2010; Buz et al., 2017; Cousin et al., 2017;

Figure 11. Two examples of the light-dark-light tonality transition. Each example shows the tonality as observed in a CTX mosaic, the corresponding CRISM spectral parameter map (red: BD1900, green: BD2100, blue: SINDEX), the final CRISM-based mineral map, and relevant spectra (locations marked in the mineral map). (a) Northwestern Mt. Sharp and associated spectra (5 × 5 pixel averages from CRISM image FRT0001BBA1 with the following central pixel locations: a1. 410, 85; a2. 452, 92; a3. 353, 66; a4. 470, 172). (b) Southwestern Mt. Sharp and associated spectra (5 × 5 pixel averages from CRISM image FRT00018C29 with the following central pixel locations: b1. 287, 332; b2. 276, 284; b3. 188, 435; b4. 287, 413; b5. 336, 348; b6. 316, 406). (c) Schematic of the mineral stratigraphy of light-dark-light transition that is exposed in various locations across lower Mt. Sharp; arrows indicate that the apparent thickness of the kieserite layer is variable. CTX, Context Camera; CRISM, Compact Reconnaissance Imaging Spectrometer for Mars; PHS, polyhydrated sulfate.

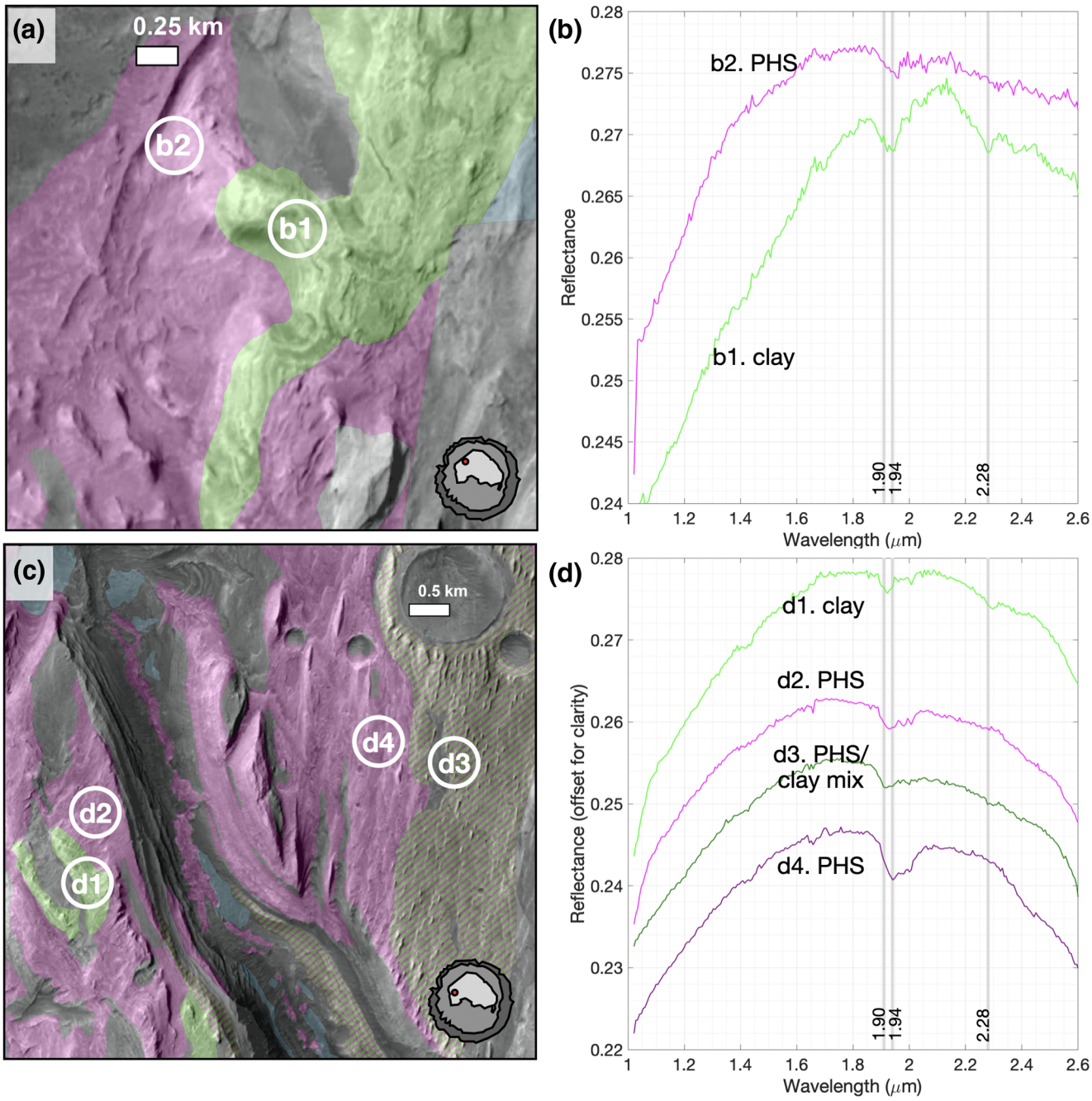

Figure 13. Two examples of locations where the clay mineral spectral signature appears to cut across or not be confined by stratigraphic boundaries. (a and b) northwest Mt. Sharp and (c and d) western Mt. Sharp on the north end of the "grand canyon." (a and c) CRISM-based mineral maps, right: spectra with relevant absorptions highlighted. (b and d) Spectra are unratioed 5 × 5 averages with the following central pixel locations: b1 [FRT00017327] 60, 414; b2 [FRT00017327] 128, 425; d1 [FRT000095EE] 396, 79; d2 [FRT000095EE] 417, 125; d3 [FRT000095EE] 195, 276; d4 [FRT000095EE] 253, 276. CRISM, Compact Reconnaissance Imaging Spectrometer for Mars.

Ehlmann & Buz, 2015). In some locations, the mafic signatures are mixed with spectral signatures of clay minerals, although it is unclear if this is due to both components being mixed within the bedrock or if it is the result of a thin covering of mafic debris (basaltic sand) on clay-bearing bedrock.

The spectrally bland class is characteristic of the Upper formation (where covered in the CRISM data used for this study), though some regions of the Lower formation, particularly those in the northeast, are also

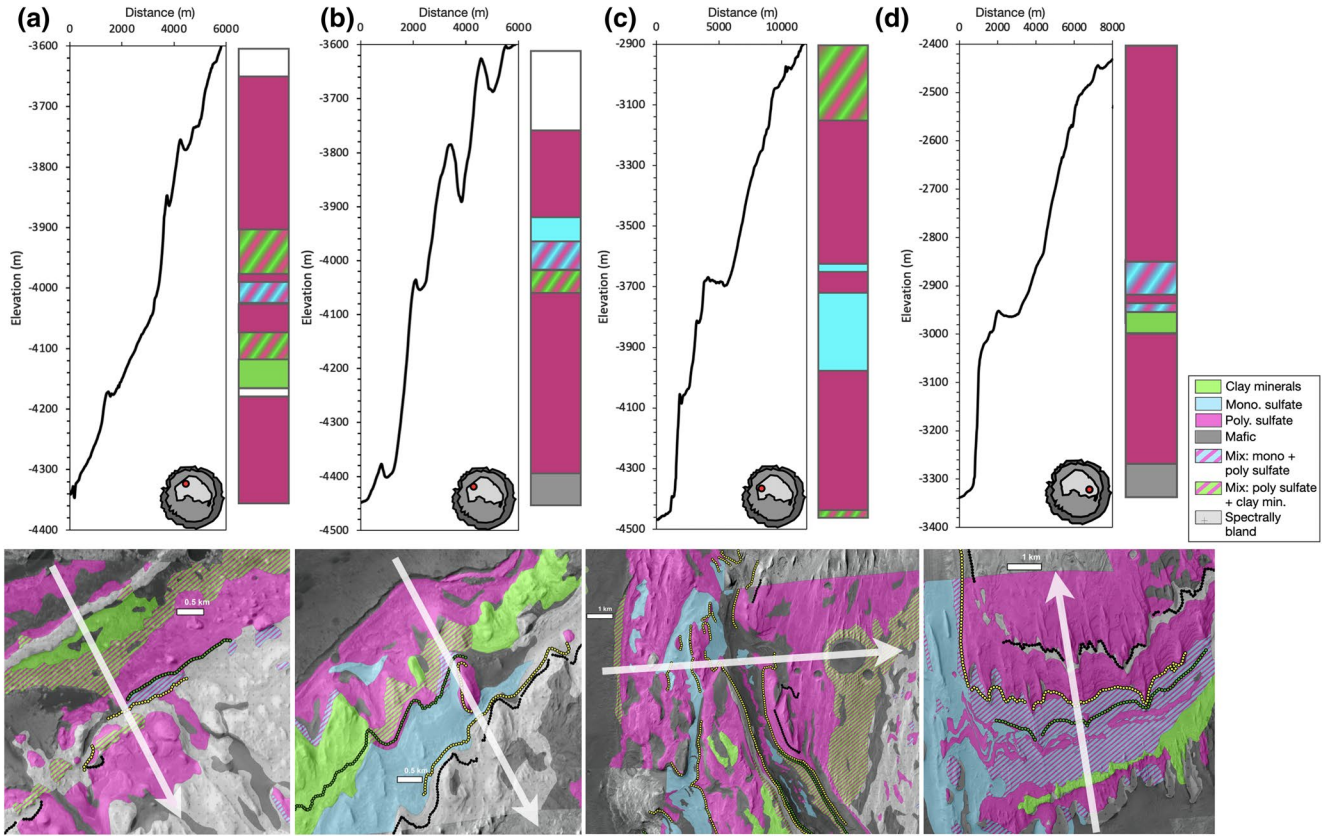

Figure 14. Example mineral stratigraphic columns from four different locations across lower Mt. Sharp (based on the CRISM-derived mineral maps and image-based DTMs). Panels (a–d) each contain the elevation profile, mineral stratigraphic column, and a closer view of the mineral map in which the transect is highlighted with a white bar and arrow pointing upsection. (a) Northwest Mt. Sharp near the planned rover traverse (white line). (b) Northwest Mt. Sharp, west of the rover traverse region. (c) Western Mt. Sharp across the "grand canyon." (d) Southeast Mt. Sharp. Similar mineral signatures and/or assemblages are observed in different locations across Mt. Sharp, but the absolute elevations of some of these signatures is highly variable. CRISM, Compact Reconnaissance Imaging Spectrometer for Mars; DTMs, digital terrain models; PHS, polyhydrated sulfate.

mapped as this class (Figures 13d and 13e). The latter may be due to bedrock being covered by dust or other talus, but it is intriguing that some portions in northeast Mt. Sharp also exhibit spectra consistent with PHS and other undifferentiated hydrous phases (Figures 13d and 13e). Spectra of the marker bed are also generally spectrally bland, but some exposures may be consistent with very weak mafic, PHS, or undifferentiated hydrous spectral signatures. As a whole, the composition of the marker bed remains enigmatic, but it is possible that it contains both primary (mafic) and secondary (sulfate/clay) minerals.

The material classified as undifferentiated hydrous is found in a range of stratigraphic positions, and it is almost always surrounded by spectrally bland material. In C518 and 20AC4, the undifferentiated hydrous areas are in the crater floor. In B6F1, 1BBA1, 17D33, and 2376B, the undifferentiated hydrous areas are stratigraphically higher, occurring within Mt. Sharp. In 1BBA1, the undifferentiated hydrous area abuts a clay-rich area, but in every other occurrence, it is fully surrounded by spectrally bland material.

5. Discussion

5.1. Composition of Hydrous Phases in Mt. Sharp

The mineralogical mapping results are consistent with previous studies that demonstrated clays and sulfates are the primary hydrous phases in Gale crater. We see no clear evidence for zeolites, perchlorates, hydrous chloride salts, or carbonates. The undifferentiated hydrous material may contain such phases, but based on their stratigraphic position and the mineralogy of nearby units, we believe they are more likely to

represent obscured clay mineral and/or sulfates signatures. The type, distribution, and possible formation conditions of the sulfates and clay minerals are discussed below.

5.1.1. Sulfates Compositions and Implications

The spectral signatures that we interpret as evidence for sulfates in Mt. Sharp are most consistent with Mg-sulfates or possibly mixed-cation sulfates such as bloedite. From an orbital perspective, there is no clear indication of sulfates in Mt. Sharp that would suggest highly acidic conditions (e.g., Al^{3+} and/or Fe^{3+} sulfates). Although jarosite ($KFe_3^{3+}(SO_4)_2(OH)_6$) has been detected in several mudstones examined by Curiosity, its abundance in the bulk rock is small relative to other hydrous mineral phases (Rampe et al., 2017) and, at least in one case, it appears to be a younger (~2.5 Ga) secondary precipitate (Martin et al., 2017). Similar to kieserite, spectra of the monohydrated ferrous sulfate szomolnokite also exhibit absorptions near ~2.1 and 2.4 μm. However, this phase is expected to oxidize if exposed at the surface of Mars (King & McSween, 2005), and spectra in regions consistent with the presence of a monohydrated sulfate do not exhibit ferrous/ferric absorption features that indicate Fe-sulfates (Mangold et al., 2008). This suggests that fluids in Gale crater during the emplacement and subsequent diagenesis of the middle and upper members of the Lower fm. may have been at circum-neutral pH, thus precluding the formation of aluminous or ferrous sulfates, or that Al^{3+} and Fe^{3+} were not abundant enough in solution to produce significant amounts of these sulfate phases.

It is notable that we do not observe any clear spectral evidence for hydrated Ca sulfates such as bassanite or gypsum. Both phases (as well as anhydrite, which cannot be detected using near infrared reflectance spectroscopy) have been identified in situ by the Curiosity rover along its entire traverse path. These Ca-sulfates most commonly occur as veins, fractures, cements, and alteration halos indicative of low water-to-rock conditions (L'Haridon et al., 2018; Nachon et al., 2017; Rampe et al., 2017; Rapin et al., 2016; Yen et al., 2017). Given how ubiquitous they are from the rover perspective, the apparent absence of these phases in the orbital data is rather enigmatic. Although they are abundant in the Murray fm., it is possible that the Ca-sulfate veins seen by Curiosity are simply too small to make up an areally significant fraction of the bedrock when viewed from orbit, resulting in a spectral dilution effect. Alternatively, some of the Ca-sulfate identified in CheMin XRD patterns is found to occur as anhydrite, which would not be detectable in CRISM data. Furthermore, the optical surface of the Ca-sulfate may have dehydrated to anhydrite under the current atmospheric conditions in Gale, which would make it invisible to CRISM, while just below the optical surface the sulfate may remain hydrated as bassanite or gypsum. Indeed, some multispectral data collected by Curiosity of veins in Yellowknife Bay show spectral evidence for gypsum at the optical surface (Nachon et al., 2014; Rice et al., 2013), providing a foundation for such veins to exist in Mt. Sharp, as well, which is in a similar temperature, pressure, and relative humidity environment. ChemCam laser ablation measurements would be able to probe this deeper hydrated Ca sulfate. This scenario could reconcile the lack of hydrated Ca sulfate seen from orbit with the occurrence of hydrated Ca sulfate observed in ChemCam data (Nachon et al., 2017; Rampe et al., 2017; Rapin et al., 2019; Vaniman et al., 2018; Yen et al., 2017).

If correct, the apparent predominance of Mg-sulfate phases in lower Mt. Sharp would be indicative of highly saline conditions given that these minerals are highly soluble (Tosca et al., 2008). Perhaps most intriguing is that the CRISM data suggest multiple hydration states of $MgSO_4 \cdot nH_2O$ ($n = 1$ and $n > 1$) may be present at the modern surface of Mt. Sharp, even though these surface materials experience similar pressure, temperature, and percent relative humidity (%RH) conditions in the current climate when they are exposed at similar elevations. The presence of two different hydration states of Mg sulfate, at least one of which appears to be stratigraphically confined (the darker, ~30–250 m thick kieserite zone of the middle member), has the potential to record important information on depositional, diagenetic, and/or erosional conditions in Gale crater.

As an example, laboratory experiments have shown that polyhydrated Mg-sulfate can form from the hydration of kieserite by increasing %RH (Vaniman et al., 2004), and this process could explain the presence of both phases in Gale crater. However, Curiosity rover environmental monitoring station observations indicate that %RH in Gale crater is generally very low (Martin-Torres et al., 2015; Rivera-Valentin et al., 2018), and previous studies deemed this process unlikely to occur for deposits in Valles Marineris where repeat Observatoire pour la Minéralogie, l'Eau, les Glaces et l'Activité and CRISM spectral observations over the

same area showed no change in sulfate hydration state over 2 martian years (Roach et al., 2009). The apparent stability of kieserite at the surface of Mars is consistent with the sluggish hydration reaction rates that have been observed for kieserite in experiments conducted under Mars-like conditions (Chipera & Vaniman, 2007; Vaniman & Chipera, 2006; Vaniman et al., 2004). Alternatively, and given the low %RH conditions throughout much of the year in Gale crater, it is more likely that higher hydration states of Mg sulfate (e.g., epsomite, hexahydrite, etc.) would dehydrate to lower hydration states under modern surface conditions. This has been examined in laboratory studies that have shown that dehydration of crystalline polyhydrated Mg-sulfates under martian conditions forms a metastable $MgSO_4 \cdot nH_2O$ phase that is XRD amorphous and polyhydrated (likely $1<n<2$) rather than dehydrating to kieserite (Chipera & Vaniman, 2007; Vaniman & Chipera, 2006; Vaniman et al., 2004). Given these constraints, different formation mechanisms or exposure histories are likely required to explain the surface occurrences of both kieserite and PHS in Gale, particularly as seen in the alternating polyhydrated and kieserite rich layers in CRISM image 17D33 in southeastern Mt. Sharp (Figure 12).

Kieserite forms under rather limited conditions, and its continued presence at the modern surface indicates these units have not been exposed to prolonged high humidity (e.g., frost or ice cover) since their formation. Or, if they were, then the higher hydration states that would have been formed at their surfaces have since been eroded away to reveal the underlying original kieserite phase. The observation that kieserite persists in what appear to be unconsolidated sediments, which presumably have high surface area and thus would be more susceptible to rehydration, also suggests kieserite is relatively stable in the modern surface environment of Gale crater. Indeed, these unconsolidated kieserite-bearing sediments may be sourced from the coherent, dark-toned strata such as the kieserite zone of the middle member. The presence of kieserite can also be informative of the humidity conditions that the strata have experienced as it is unlikely to form as a direct dehydration product of crystalline polyhydrated $MgSO_4 \cdot nH_2O$ ($n = 2,4,5,6,7$). The darker-toned kieserite zone of the middle member, for example, may represent and record ancient aqueous processes that are distinct from the PHS-bearing strata above and below it.

In contrast with the kieserite occurrences, attempting to infer the aqueous history of the PHS-bearing strata may be more complex. As noted above, it is possible that the PHS may be an X-ray amorphous product formed by the dehydration of what was formerly a crystalline $MgSO_4 \cdot nH_2O$ phase (e.g., epsomite, hexahydrite, pentahydrite, etc.), or it could still be one of these crystalline forms (with $n>1$). Distinguishing between these possibilities using near-IR reflectance data is difficult, particularly from orbit at the spectral resolution and signal level of the CRISM data. In either case, whether the PHS is X-ray amorphous or crystalline, experimentally determined stability fields for the $MgSO_4 \cdot H_2O$ system (Chipera & Vaniman, 2007; Chou et al., 2013; Vaniman & Chipera, 2006; Vaniman et al., 2004; Wang et al., 2006, 2016) suggest the conditions that would result in varieties of Mg PHS would be distinct from those that resulted in the kieserite-bearing strata. However, the relative ease at which $MgSO^4$ can cycle between some of these hydration states (and crystalline vs. amorphous states) (Chipera & Vaniman, 2007; Vaniman & Chipera, 2006) indicates that the current hydration state of the PHS is likely to be more indicative of modern environmental conditions (P, T, %RH) rather than a recorder of properties of the fluid from which the Mg sulfate originally precipitated.

5.1.2. Clay Mineral Compositions and Implications

The occurrences of clay minerals observed from orbit are largely consistent with Fe-rich varieties such as nontronite, suggesting they are products formed by dissolution of primary Fe-rich minerals (e.g., olivine and pyroxene). As described above, there is some variation in clay mineral composition suggested by subtle differences in the metal-OH band position (Figures 8 and 14). The metal-OH band is centered at 2.28–2.29 μm in the majority of the clay mineral spectra in Mt. Sharp (Figures 14d, 14e and 14g), suggestive of Fe-rich smectite (e.g., nontronite) with minor Mg^{2+} substitution into the octahedral sheet (Bristow et al., 2018; Michalski et al., 2015). In a few locations, most commonly in the crater floor, the metal-OH absorption is shifted to a longer wavelength position of ~2.3 μm (Figure 8), a position that is indicative of an increase in Mg^{2+} content. These spectra are consistent with either Fe/Mg-smectite or perhaps a mixed layer chlorite-smectite. The apparent different cation chemistry of these clay minerals suggests they are from a distinct source region (if they are detrital) or that they have resulted from or been exposed to processes that

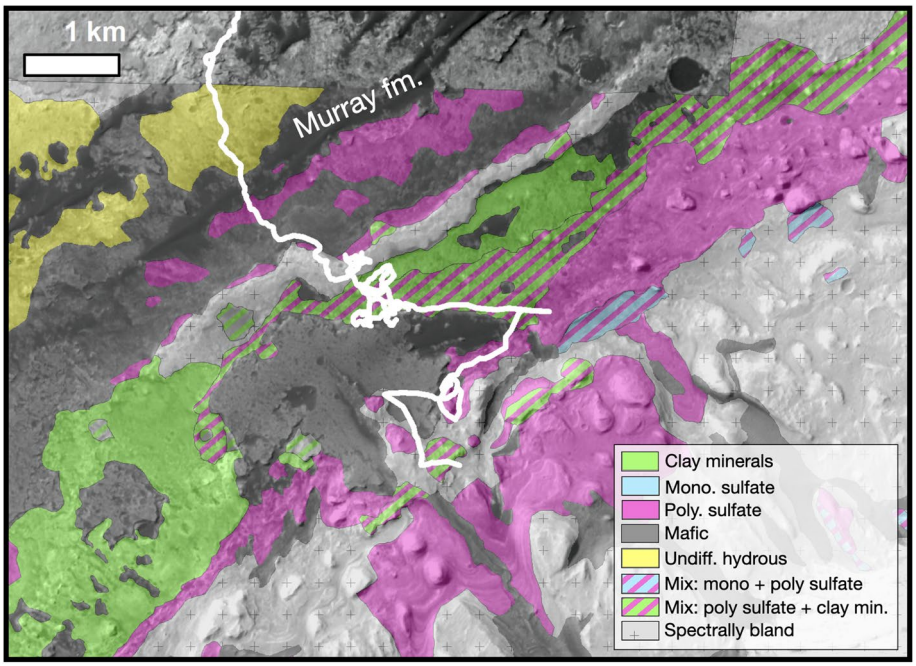

Figure 15. CRISM-based mineral map overlain on CTX mosaic and highlighting the traverse route of the Curiosity rover.

resulted in higher Mg concentrations. From orbit, there is no obvious evidence for large exposures of Al-rich clay minerals (e.g., montmorillonite, illite, kaolinite) or chlorite in lower Mt. Sharp. These observations of the clay minerals in Gale crater are consistent with alteration in the presence of water and oxidation of iron, though whether such alteration took place on the surface or in the subsurface is unclear from orbital data (Bristow et al., 2018; Michalski et al., 2015).

The CheMin XRD data provide an opportunity to compare the mineralogy observed in situ with predictions made from orbital spectroscopy. The scale of data collection complicates direct comparison, however: CheMin analyzes just a few grams of powder from a drill hole centimeters below the surface, while CRISM is sensitive to the upper few micrometers of large spatial areas. The primary clay-bearing region along the rover traverse path (in the Glen Torridon region) was suggested to be Fe-rich (nontronite) with possible substitution of Al^{3+}, and CheMin data have confirmed this to be the case (Bristow et al., 2019). However, clay minerals have been observed in all mudstone samples analyzed by CheMin to date (Bristow et al., 2018, 2019; Rampe et al., 2017), some of which were collected in areas with no clear indications of clay minerals in the orbital data and others collected in areas mapped as "undifferentiated hydrous" in this study (Figure 15). Examples of the former indicate that the distribution of clay minerals in Mt. Sharp is likely underestimated based solely on orbital data, and the latter examples suggest that some clay-bearing outcrops may exhibit weak H_2O absorptions in orbital spectra but lack the weaker metal-OH features that are required for diagnostic identification of clay minerals. It is possible, therefore, that other areas mapped as undifferentiated hydrous are also clay-bearing, with some characteristic of the setting (e.g., dust cover, diagenetic overprinting, mixing with other phases) obscuring the weaker metal-OH features in the orbital spectra.

5.2. Stratigraphic Variations in the Mineralogy of Mt. Sharp

A first order question in determining whether hydrated minerals in Mt. Sharp are related to local, regional, or global conditions is whether or not they are detrital or authigenic components. This question cannot be definitively answered using only orbital data, but before exploring the necessary in situ observations to determine their origin, we first describe our main orbital interpretations of the mineral stratigraphy and the possible associated formation conditions.

First, the light to dark to light vertical tonality transitions that are traceable around Mt. Sharp correspond to the same mineralogical transitions wherever they are seen, and these tonality changes appear to conform to bedding. This transition is essentially a discrete, consistent kieserite zone embedded within a thick sequence of PHS. These sulfates could be detrital, but because most sulfates, and Mg sulfates in particular, are relatively soluble, it is extremely unlikely that the PHS and kieserite represent transported materials. If they are instead authigenic phases, then they may represent either primary chemical precipitates or diagenetic phases. If they are diagenetic then the sulfates may have formed early, shortly after deposition of detrital components and perhaps near a sediment-water interface. If we see chemical signatures and color changes that cut across laminations and bedding, that would be indicative of diagenetic processes (Frydenvang et al., 2017). Alternatively, they may be late diagenetic features, forming after lithification of host sediments. If the kieserite is assumed to reliably preserve information about the fluids from which it initially precipitated (i.e., not affected by subsequent hydration-dehydration reactions), and if it is found to occur as evaporite beds or as an early diagenetic phase, then it would be an important recorder of aqueous conditions at or very near the time of sediment deposition. For example, the entire sulfate package (mono- and polyhydrated) may be fully lacustrine, with the kieserite strata recording a change in lake geochemistry.

Another possibility is that the PHS may be sulfate cemented sandstone (e.g., Milliken et al., 2014), with the kieserite recording a lake horizon sandwiched by complex nonlacustrine PHS-rich strata. In this scenario, the widespread occurrence of the kieserite zone suggests a lake or series of contemporaneous lakes would likely have filled the entire crater during the period of kieserite formation, possibly with drier climates before and after leading to nonlacustrine deposition of the PHS-bearing units. The transition to these drier periods may have involved a period of multiple smaller lakes, either isolated or interconnected by streams, as proposed in Rapin et al. (2019). The sulfate sequence could also be the result of late stage diagenesis, reflecting younger aqueous processes, possibly many millions of years after the time of sediment deposition; there is evidence for diagenetic processes in this area (Siebach & Grotzinger, 2014; Sun et al., 2019). In this diagenetic case, the stratigraphic boundaries of the kieserite would be controlled by porosity and permeability.

The thinner alternating kieserite and PHS layers in southeastern Mt. Sharp (Figure 12c) have many of the same possible formation mechanisms as outlined above for the larger scale light-dark-light tonality transitions found around Mt. Sharp. The layers may be truly interbedded, having formed by alternating brine chemistry during deposition, or they could represent differences in diagenetic and/or weathering processes. As an example of the latter, the alternating PHS-kieserite layers could once have been a single sequence of kieserite in which some layers have hydrated to PHS. Although this reaction is sluggish, even at high %RH (Chipera & Vaniman, 2007; Vaniman et al., 2004), it is possible that physical attributes of some layers (porosity, grain size, degree of cementation, etc.) may promote or prohibit hydration compared with other layers. The kieserite-bearing layers, for example, may erode more rapidly than the rate at which kieserite can hydrate, whereas the PHS layers may be more competent and thus remain intact long enough for kieserite to convert to PHS. However, this scenario may be unlikely given that the hydration reaction is accompanied by a volume expansion that would be more likely to increase erosion or sloughing off of materials exposed at the faces of the PHS layers. In addition, we observe no strong variations in surface slopes of the kieserite versus PHS layers that would indicate significant differences in their rates of erosion. The Curiosity rover will not explore these southeastern layers, but it is possible that the alternating PHS-kieserite layers are continuous through Mt. Sharp and are only resolvable in CRISM and HiRISE data in the SE because of the lower vertical relief. Searching for similar alternating patterns as the rover ascends through the lower sulfate unit in NW Mt. Sharp may help determine the origin of these strata.

Another key finding of this work is that clay minerals are found in multiple stratigraphic positions, they occur as thinner units than PHS-bearing strata, and individual occurrences are not laterally extensive. This is a critical point concerning the clay mineral spectral signatures stratigraphically above what Curiosity has explored. Existence of clay minerals spanning a wide stratigraphic range suggests that, within Gale crater at least, a transition from clay mineral dominated to sulfate dominated conditions was more protracted (to the extent in which thicker strata means more time) than previously recognized. Local formations in the Gale environment occurred for longer than previously recognized and any transition to sulfate forming period spanned longer amounts of time. Though the relative stratigraphic positions of clay mineral exposures

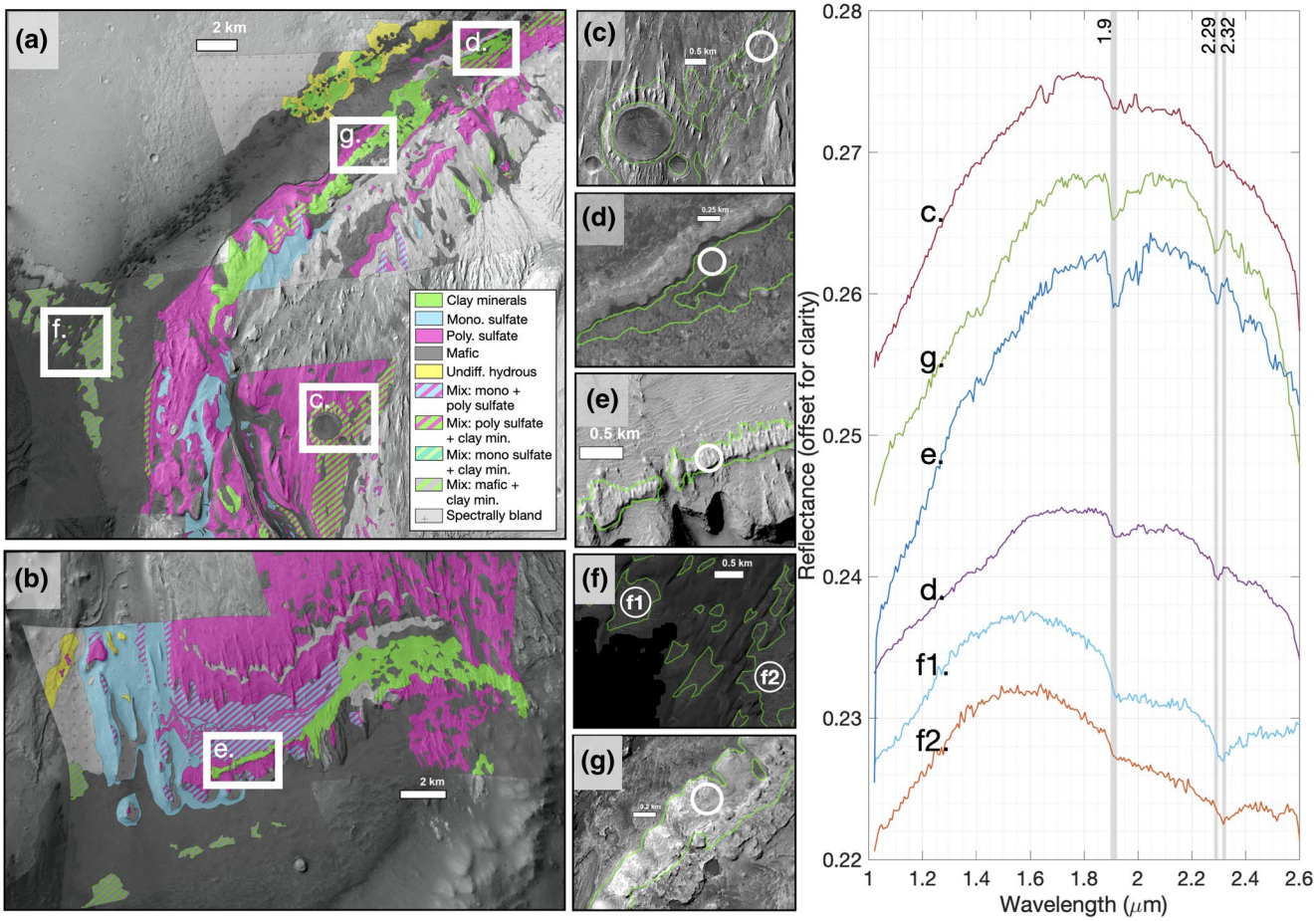

Figure 16. Clay minerals are detected in multiple stratigraphic positions in lower Mt. Sharp and exhibit a range in visible morphology. Example exposures along (a) northwestern and (b) southeastern Mt. Sharp. (c) Mix of PHS and Fe-Mg clay mineral, stratigraphically higher than the clay-bearing unit explored by Curiosity and depicted in the stratigraphic column of Milliken et al. (2010) that is shown in Figure 1. (d) Fe-Mg-bearing clay minerals in the Glen Torridon region (clay-bearing unit), considered stratigraphically "low." (e) Somewhat erosionally resistant Fe-Mg clay-bearing cliffs in southeast Mt. Sharp, considered stratigraphically "low." (f) Additional Mg-rich clay minerals mixed with mafic sediment (sand), stratigraphically lower than the Glenn Torridon clay-bearing unit. (g) A more erosionally resistant clay-bearing zone in the northwest, stratigraphically "low" and likely stratigraphically analogous to the Glenn Torridon region shown in (d). Spectra are unratioed 5 × 5 averages with the following central pixel locations: c [FRT000095EE] 61, 414; d [FRT0000B6F1] 343, 416; e [FRT00017D33] 178, 201; f1 [FRT00017327] 574, 417; f2 [FRT00017327] 436, 355; g [FRT0001BBA1] 222, 272. PHS, polyhydrated sulfate.

share similarities (e.g., there are several occurrences below the kieserite zone), it is not possible to correlate a given clay mineral exposure to another one over very long distances. This suggests that although clay minerals are present in many places in lower Mt. Sharp, the nature of the clay minerals is laterally discontinuous around the mound (i.e., their presence, abundance, or intermixing with other minerals that affects their visibility from orbit). Differentiating between detrital versus authigenic emplacement mechanisms is particularly difficult for clay minerals, which are rather insoluble and could easily be transported by fluvial (or eolian) processes, or which could be produced antigenically in a lacustrine environment or by diagenetic fluids. Orbital observations of the lateral and vertical distribution of clay minerals in Mt. Sharp and relationships with bedding contacts can be used to help determine which of these scenarios may be more likely than others. Unfortunately, the extensive amount of erosion and redistribution of sediment across Mt. Sharp as a whole makes it difficult to determine with certainty whether the clay mineral spectral signatures crosscut or conform to stratigraphic boundaries. However, two examples of what appear to be lateral and/or vertical transitions between clay mineral and PHS signatures are shown in Figure 16. In the first (Figure 16a), located in NW Mt. Sharp, an area rich in clay minerals appears to pinch out and transition laterally into PHS. In the second example (Figure 16b), PHS spectral signatures transition to pure clay mineral spectral signatures on one side of the Mt. Sharp "grand canyon," whereas on the other side of the canyon, it transitions

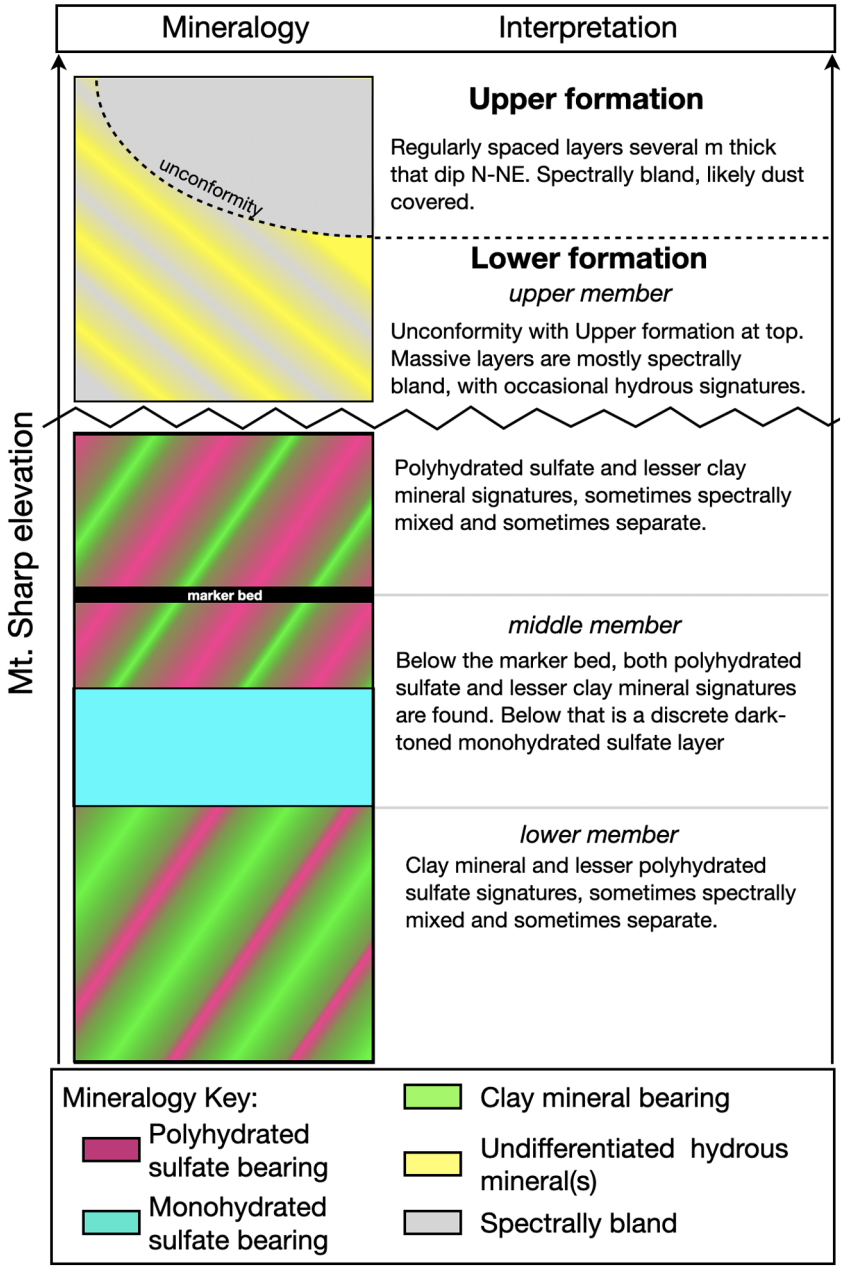

Figure 17. Schematic of the interpreted mineral stratigraphic column of Mt. Sharp based on HiRISE images and the processed CRISM images presented here. This represents an update of the mineral stratigraphic column presented in Milliken et al. (2010) (Figure 1c). The Upper formation is spectrally bland. The Lower formation has three orbitally defined members: upper, middle, and lower. The lower member contains the strongest signatures of Fe/Mg clay minerals with lesser signatures of PHS, and the Curiosity rover has only traversed regions within the lower member. The transition from lighter to darker-toned strata marks the upper boundary of the lower member. The middle member is dominated by darker-toned strata that appear to be enriched in monohydrated Mg sulfate. This member is quite variable in thickness (e.g., Figure 6) and in some locations the upper boundary of the dark-toned zone coincides with the marker bed, whereas in other regions they are separated by a distinct section of PHS/clay-bearing strata. The latter case is depicted in this figure, whereas the former case was depicted in the column of Milliken et al. (2010) as shown in Figure 1c. Because it remains a distinct, traceable, tie point, the marker bed is still used to mark the upper boundary of the middle member. The lower portions of the upper member exhibit spectral signatures of PHS and less frequent occurrences clay minerals, whereas the uppermost portions of the upper member are commonly spectrally bland, with minor undifferentiated hydrous signatures. The nature and origin of the transition between the hydrated phases and the spectrally bland region is not clear from orbital data, and the bland areas may simply be due to increased dust cover in the upper regions of the upper member. CRISM, Compact Reconnaissance Imaging Spectrometer for Mars; HiRISE, High Resolution Imaging Science Experiment; PHS, polyhydrated sulfate.

to spectrally mixed clay mineral/PHS. In neither case is there evidence of a clear stratigraphic boundary that corresponds with these spectral changes, rather the changes appear to crosscut bedding. Though not definitive, these examples would be consistent with the concept that at least some clay minerals in Gale crater are the result of authigenitic/diagenetic processes (Bristow et al., 2018; Vaniman et al., 2014). Given the variable nature of the relative proportion of clay minerals and PHS within lower Mt. Sharp, and the lack of clear stratigraphic boundaries between clay- and PHS-rich units, it is possible that clay mineral and PHS phases are both present throughout the strata immediately below and above the kieserite section and that their abundances vary laterally throughout these strata.

Based on these results, we present an interpreted mineral stratigraphic column for Mt. Sharp as a whole (Figure 17). This is an updated version of the column from Milliken et al. (2010), now generalized for the entirety of the sedimentary mound rather than focused on the northwest.

5.3. Relevance to Upcoming Rover Observations

Current and future observations by the Curiosity rover have the potential to test some of the possible formation conditions discussed above and shed light on the depositional environments and histories associated with these materials. To achieve this goal, some of the most important things to constrain with detailed in situ documentation would be (1) the mineralogy, chemistry and textural attributes (grain size, scale of bedding, possible crystal molds/bottom growth textures, etc.) of the laterally continuous kieserite band and its host PHS strata (Figure 12c), and (2) the spatial extent, chemistry, and sedimentology of the more laterally discontinuous clay-bearing strata, including relationships to stratigraphic contacts that may be observable from orbit.

Determining whether the sulfates in Mt. Sharp are primary or diagenetic requires rover-scale observations of whether the transitions conform to stratigraphic boundaries, the textural attributes of the strata, and occurrence relative to other components in the rocks. The generally through-going nature of these mineralogical zones and their associated morphologies suggests that whatever process created them occurred throughout Mt. Sharp. This suggests that at least some processes documented along the rover traverse are applicable to the crater environment as a whole. Curiosity will approach these sulfate transitions during its extended mission, offering the opportunity to observe these mineralogical changes in situ. A challenge is that the dark kieserite zone is pervasive throughout Mt. Sharp but poorly expressed near the rover traverse due to significant erosion. The most promising potential exposure that could be examined in situ is shown in Figures 18c and 18e. In this location, there exists a darker-toned band that is overlain by lighter-troned strata with weak PHS and Fe/Mg-clay mineral spectral signatures. (Figure 18e, locations 1 and 2). The few CRISM pixels over the dark band itself are consistent with a spectral mixture of PHS and weak kieserite. Stratigraphically below the dark band is PHS and below that the Fe-rich clay mineral strata of the Glen Torridon region. These observations are consistent with this being an eroded exposure of the light-dark-light sulfate package, and as such it constitutes the best opportunity to observe these mineral transitions in situ.

If the sulfates are direct chemical precipitates produced by evaporation of surface waters, such as in a shallow lake or playa environment, the rover payload could be used to look for textural evidence such as thin, salt-rich evaporite beds, bottom growth crystal structures, or perhaps sulfate rich clastic deposits indicative of evaporative concentration (i.e., dirty evaporites). Such small-scale textural features can be observed with the rover payload as described in (Kah et al., 2018), where lenticular features are identified as primary gypsum formed in the shallow subsurface. If they are diagenetic, determining whether they are the cementing agent in a sandstone or mudstone versus thin beds would help constrain their formation time. Diagenetic layers would be more diagnostic of variations in porosity and permeability. Diagenetic fluid flow would be affected by bedding boundaries, so it could closely align with bedding. Observations that may help estimate grain size would also be informative: if sulfates are observed in more resistant or cliff forming units, they may be coarser grained or more strongly cemented sandstones.

Unlike the sulfate-rich strata, the clay minerals documented by the rover are not laterally continuous through Mt. Sharp. While this could be affected by dust cover masking clay mineral signatures, local slopes are similar to the areas with discernible, continuous sulfate signatures making variable dust cover an unlikely origin of this observation. It is also possible clays are laterally continuous but physical mixtures with

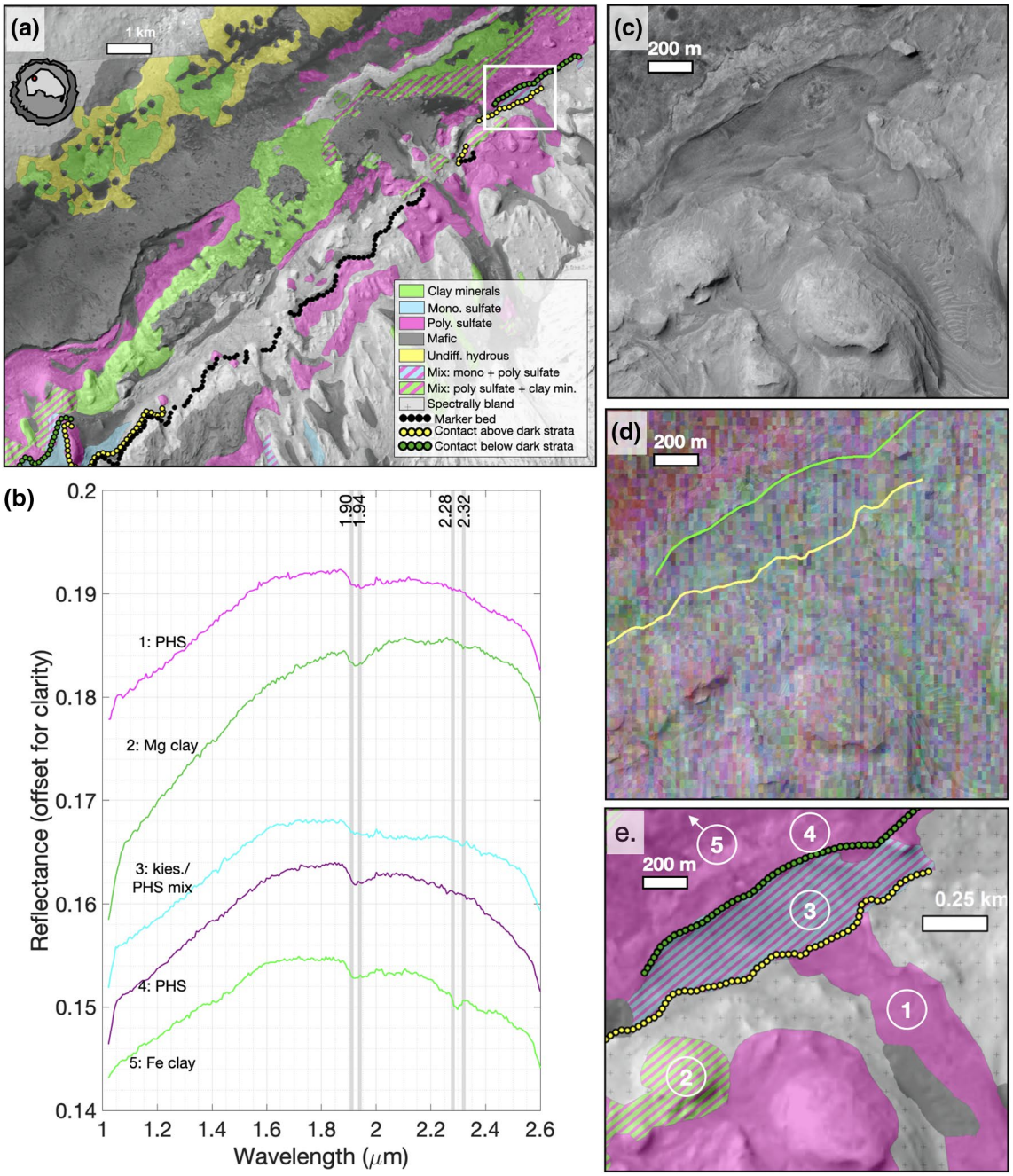

Figure 18. Details of the CRISM-based mineralogy in the area closest to the planned rover traverse route indicating where the light-dark-light PHS-kieserite-PHS transition might be exposed. (a) Mapped mineralogy of this area (image FRT0000B6F1). White box shows the location of panels (c–e). (b) Relevant 5 × 5 average, unratioed spectra (b1: PHS, b2: Mg-rich phyllosilicate, 3: kieserite/PHS mix, 4: PHS, 5: Fe-rich phyllosilicate). (c) HiRISE image, (d) CRISM spectral parameter map (red: BD1900, green: BD2100, blue: SINDEX), and (e) close-up of mineral map marked with locations of spectra presented in (b). Spectra are unratioed 5 × 5 averages with the following central pixel locations in [FRT0000B6F1]: 1. 258, 347; 2. 305, 332; 3. 286, 371; 4. 291, 388; 5. 343, 416. CRISM, Compact Reconnaissance Imaging Spectrometer for Mars; HiRISE, High Resolution Imaging Science Experiment; PHS, polyhydrated sulfate.

other minerals (e.g., Mg sulfates) leads to overlapping spectral features that obscures the presence of clay minerals in some areas based on the relative proportion. This possibility cannot be eliminated at this time, and more in situ observations of clay mineral mixtures will help determine the likelihood of such mixtures as a way to explain clay minerals detected in situ in places they have not been seen from orbit. If the clay minerals truly are not continuous, however, there are implications for either the primary lacustrine or the

diagenetic aqueous setting. The chemistry of clay minerals in the Glen Torridon clay-bearing unit seems to be in line with clay minerals observed elsewhere in Mt. Sharp, although the discontinuity of clay mineral zones suggests that lakes within Gale may have been smaller or discontinuous, not necessarily crater-wide. If the clay minerals throughout Mt. Sharp are predominantly diagenetic, the fluids that produced them may have had similar properties that resulted in similar clay mineral types and chemistry. However, because the occurrences of clay-bearing strata are not continuous at the orbital scale, the environmental conditions and processes inferred for clay minerals along the rover traverse may not be entirely transferable to other clay-bearing areas in Mt. Sharp. There is evidence for multiple clay mineral occurrences throughout the Lower formation, so clay minerals are likely to continue to be present within the sulfate-bearing unit; these clay minerals may occur as discrete beds or intimately mixed with sulfates.

6. Conclusions

Our updated assessment of orbital near-infrared reflectance spectra continues to support the concept that the major mineral stratigraphy of Mt. Sharp is one in which clay-bearing strata are abundant in the lowest portion of Mt. Sharp (e.g., the Murray fm.) and are overlain by a more sulfate-rich section. However, clay mineral and sulfate strata are not mutually exclusive. Though the previously recognized "sulfate" unit is spectrally dominated by sulfate when considering Mt. Sharp as a whole, it also contains zones enriched in clay minerals. In situ observations that help to identify the depositional environments associated with the mineral signatures observed from orbit, and the hydrated phases in particular, will help determine the extent to which conclusions about the environment along Curiosity's traverse can be extrapolated to other locations in Mt. Sharp and possibly beyond. Because of their apparent laterally discontinuous nature, some of the clay mineral signatures observed in orbital data of Mt. Sharp may be more reflective of local conditions and fluid compositions rather than conditions typical of the entire crater environment. As such, the occurrence of clay minerals at multiple locations in Mt. Sharp is not sufficient evidence to conclude that processes and conditions leading to clay mineral formation/deposition at one location are applicable to other clay-bearing zones in the mountain.

In contrast to the clay mineral signatures, the spectral and tonal characteristics associated with the darker-toned kieserite zone of the middle member are remarkably consistent, stratigraphically confined, and traceable over longer distances. This suggests the darker kieserite zone is a coherent package of strata that is present through most if not all of Mt. Sharp. Rover-based observations and interpretations for this unit may reflect processes and/or conditions that applied to the entirety of Gale crater. Despite its apparently through-going nature, the large variations in elevation and thickness of the dark toned kieserite zone remain enigmatic and warrants additional study, especially given that there is currently no clear evidence for large scale faulting in lower Mt. Sharp. Rover-scale observations on the distribution, chemistry, and hydration state of sulfates in lower Mt. Sharp can help constrain the depositional conditions associated with the polyhydrated and monohydrated sulfate units, including differentiating primary versus secondary (diagenetic) processes. Because a number of other craters appear to have been partially or completely filled, lithified, and significantly eroded (Malin & Edgett, 2000; Thomson et al., 2011), differentiating between local and crater-wide processes recorded in the strata of Mt. Sharp is informative not only for Gale crater but also for constraining interpretations of other craters on Mars that host central mounds.

Data Availability Statement

The processed CRISM remote sensing data used in this work are publicly available in Milliken (2020), https://10.26300/2q8p-wb51.

Acknowledgments
We would like to acknowledge funding from the NASA MSL Participating Scientist Program and JPL Subcontract Number 1549766. We also acknowledge the MRO CRISM, HiRISE, MSL, and CTX science teams. This work was greatly improved by helpful discussions with R. Arvidson, W. Rapin, J. Bishop, and K. Seelos, S. Ruff, and one anonymous reviewer.

References

Adams, J. B. (1974). Visible and near infrared diffuse reflectance spectra of pyroxenes as applied to remote sensing of solid objects in the solar system. *Journal of Geophysical Research*, *79*(32), 4829–4836.

Anderson, R. B., & Bell, J. F. (2010). Geologic mapping and characterization of Gale Crater and implications for its potential as a Mars Science Laboratory landing site. *The International Journal of Mars Science and Exploration*, 76–128. https://doi.org/10.1555/mars.2010.0004

Anderson, R. B., Edgar, L. A., Rubin, D. M., Lewis, K. W., & Newman, C. (2018). Complex bedding geometry in the upper portion of Aeolis Mons, Gale crater, Mars. *Icarus*, *314*, 246–264.

Bandfield, J. L., Edwards, C. S., Montgomery, D. R., & Brand, B. D. (2013). The dual nature of the martian crust: Young lavas and old clastic materials. *Icarus*, *222*, 188–199.

Banham, S. G., Gupta, S., Rubin, D. M., Watkins, J. A., Sumner, D. Y., Edgett, K. S., & Vasavada, A. R. (2018). Ancient Martian aeolian processes and palaeomorphology reconstructed from the Stimson formation on the lower slope of Aeolis Mons, Gale crater, Mars. *Sedimentology*, *65*, 993–1042. https://doi.org/10.1111/sed.12469

Bibring, J.-P., Langevin, Y., Mustard, J. F., Poulet, F., Arvidson, R., Gendrin, A., et al. (2006). Global mineralogical and aqueous Mars history derived from OMEGA/Mars express data. *Science*, *312*, 400–404.

Bishop, J. L., Lane, M. D., Dyar, M. D., & Brown, A. J. (2008). Reflectance and emission spectroscopy study of four groups of phyllosilicates: Smectites, kaolinite-serpentines, chlorites and micas. *Clay Minerals*, *43*(1), 35–54. https://doi.org/10.1029/2009JE003352

Bishop, J. L., Parente, M., Weitz, C. M., Dobrea, E. Z. N., Roach, L. H., Murchie, S. L., & Mustard, J. F. (2009). Mineralogy of Juventae Chasma: Sulfates in the light-toned mounds, mafic minerals in the bedrock, and hydrated silica and hydroxylated ferric sulfate on the plateau. *Journal of Geophysical Research*, *114*.

Bishop, J. L., Pieters, C. M., & Edwards, J. O. (1994). Infrared spectroscopic analyses on the nature of water in montmorillonite. *Clay and Clay Minerals*, *42*(6), 702–716.

Bristow, T. F., Bish, D. L., Vaniman, D. T., Morris, R. V., Blake, D. F., Grotzinger, J. P., & Mcadam, A. C. (2015). The origin and implications of clay minerals from Yellowknife Bay, Gale crater, Mars. *American Mineralogist*, *100*, 824–836.

Bristow, T. F., Rampe, E. B., Achilles, C. N., Blake, D. F., Chipera, S. J., Craig, P., & Yen, A. S. (2018). Clay mineral diversity and abundance in sedimentary rocks of Gale crater, Mars. *Science Advances*, *4*(6).

Bristow, T. F., Rampe, E. B., Grotzinger, J. P., Fox, V. K., Bennett, K. A., Yen, A. S., Achilles, C. N. (2019). *Clay minerals of Glen Torridon, Mount sharp, Gale crater, Mars*. Abstract at the Ninth International Conference on Mars, Pasadena, CA.

Burns, R. G. (1993). *Mineralogical applications of crystal field theory*, Cambridge, England: Cambridge University Press.

Buz, J., Ehlmann, B. L., Pan, L., & Grotzinger, J. P. (2017). Mineralogy and stratigraphy of the Gale crater rim, wall, and floor units. *Journal of Geophysical Research: Planets*, *122*, 1090–1118. https://doi.org/10.1002/2016JE005163

Cabrol, N. A., Grin, E. A., Newsom, H. E., Landheim, R., & McKay, C. P. (1999). Hydrogeologic evolution of Gale crater and its relevance to the exobiological exploration of Mars. *Icarus*, *139*, 235–245.

Chipera, S. J., & Vaniman, D. T. (2007). Experimental stability of magnesium sulfate hydrates that may be present on Mars. *Geochimica et Cosmochimica Acta*, *71*, 241–250.

Chou, I.-M., Seal, R. R., & Wang, A. (2013). The stability of sulfate and hydrated sulfate minerals near ambient conditions and their significance in environmental and planetary sciences. *Journal of Asian Earth Sciences*, *62*, 734–758.

Clark, R. N., King, T. V. V., Klejwa, M., Swayze, G. A., & Vergo, N. (1990). High spectral resolution reflectance spectroscopy of minerals. *Journal of Geophysical Research*, *95*(B8), 12653–12680.

Cloutis, E. A., & Gaffey, M. J. (1991). Pyroxene spectroscopy revisited: Spectral compositional correlations and relationship to geothermometry. *Journal of Geophysical Research*, *96*(E5), 22809–22826.

Cloutis, E. A., Hawthorne, F. C., Mertzman, S. A., Krenn, K., Craig, M. A., Marcino, D., & Vilas, F. (2006). Detection and discrimination of sulfate minerals using reflectance spectroscopy. *Icarus*, *184*(1), 121–157.

Cousin, A., Sautter, V., Payre, V., Forni, O., Mangold, N., Gasnault, O., & Rapin, W. (2017). Classification of igneous rocks analyzed by ChemCam at Gale crater, Mars. *Icarus*, *288*, 265–283.

Ehlmann, B. L., & Buz, J. (2015). Mineralogy and fluvial history of the watersheds of Gale, Knobel, and Sharp craters: A regional context for the Mars Science Laboratory Curiosity's exploration. *Geophysical Research Letters*, *42*, 264–273. https://doi.org/10.1002/2014GL062553

Ehlmann, B. L., Mustard, J. F., Fassett, C. I., Schon, S. C., Head, J. W., III, Des Marais, D. J., & Murchie, S. L. (2008). Clay minerals in delta deposits and organic preservation potential on Mars. *Nature Geoscience*, *1*, 355–358.

Fraeman, A. A., Arvidson, R. E., Catalano, J. G., Grotzinger, J. P., Morris, R. V., Murchie, S. L., & Viviano, C. E. (2013). A hematite-bearing layer in Gale Crater, Mars: Mapping and implications for past aqueous conditions. *Geology*, *41*(10), 1103–1106. https://doi.org/10.1130/G34613.1

Fraeman, A. A., Ehlmann, B. L., Arvidson, R. E., Edwards, C. S., Grotzinger, J. P., Milliken, R. E., & Rice, M. S. (2016). The stratigraphy and evolution of lower Mount Sharp from spectral, morphological, and thermophysical orbital data sets. *Journal of Geophysical Research: Planets*, *121*, 1713–1736. https://doi.org/10.1002/2016JE005095

Frydenvang, J., Gasda, P., Hurowitz, J., Grotzinger, J., Wiens, R., Newsom, H., & Vasavada, A. (2017). Diagenetic silica enrichment and late-stage groundwater activity in Gale crater, Mars: Silica enriching diagenesis, Gale, Mars. *Geophysical Research Letters*, *44*, 4716–4724. https://doi.org/10.1002/2017GL073323

Gendrin, A., Mangold, N., Bibring, J.-P., Langevin, Y., Gondet, B., Poulet, F., & LeMouelic, S. (2005). Sulfates in Martian layered terrains: The OMEGA/Mars Express view. *Science*, *307*(5715), 1587–1591.

Grotzinger, J. P., Crisp, J., Vasavada, A. R., Anderson, R. C., Baker, C. J., Barry, R., & Wiens, R. C. (2012). Mars Science Laboratory mission and science investigation. *Space Science Reviews*, *170*(1), 5–56. https://doi.org/10.1007/s11214-012-9892-2

Grotzinger, J. P., Gupta, S., Malin, M. C., Rubin, D. M., Schieber, J., Siebach, K., & Wilson, S. A. (2015). Deposition, exhumation, and paleoclimate of an ancient lake deposit, Gale crater, Mars. *Science*, *350*(6257).

Grotzinger, J. P., Sumner, D. Y., Kah, L. C., Stack, K., Gupta, S., Edgar, L., & Yingst, A. (2014). A habitable fluvio-lacustrine environment at Yellowknife Bay, Gale crater, Mars. *Science*, *343*.

Hurowitz, J. A., Grotzinger, J. P., Fisher, W. W., McLennan, S. M., Milliken, R. E., Stein, N., & Wiens, R. C. (2017). Redox stratification of an ancient lake in Gale crater, Mars. *Science*, *356*(922).

Itoh, Y., & Parente, M. (2021). A new method for atmospheric correction and de-noising of CRISM hyperspectral data. *Icarus*, *354*.

Kah, L. C., Stack, K. M., Eigenbrode, J. L., Yingst, R. A., & Edgett, K. S. (2018). Syndepositional precipitation of calcium sulfate in Gale crater, Mars. *Terra Nova*, *30*(6), 431–439. https://doi.org/10.1111/ter.12359

King, P. L., & McSween, H. Y., Jr. (2005). Effects of H_2O, pH, and oxidation state on the stability of Fe minerals on Mars. *Journal of Geophysical Research*, *110*(E12). https://doi.org/10.1029/2005JE002482

Kite, E. S., Lewis, K. W., Lamb, M. P., Newman, C. E., & Richardson, M. I. (2013). Growth and form of the mound in Gale Crater, Mars: Slope wind enhanced erosion and transport. *Geology*, *41*(5), 543–546.

Klima, R. L., Dyar, M. D., & Pieters, C. M. (2011). Near-infrared spectra of clinopyroxenes: Effects of calcium content and crystal structure. *Meteoritics & Planetary Sciences*, *46*(3), 379–395.

Leask, E. K., Ehlmann, B. L., Dundar, M. M., Murchie, S. L., & Seelos, F. P. (2018). Challenges in the search for perchlorate and other hydrated minerals with 2.1-μm absorptions on Mars. *Geophysical Research Letters*, *45*, 12180–12189. https://doi.org/10.1029/2018GL080077

Le Deit, L., Hauber, E., Fueten, F., Pondrelli, M., Rossi, A. P., & Jaumann, R. (2013). Sequence of infilling events in Gale Crater, Mars: Results from morphology, stratigraphy, and mineralogy. *Journal of Geophysical Research: Planets*, *118*, 1–35. https://doi.org/10.1002/2012JE004322

L'Haridon, J., Mangold, N., Meslin, P.-Y., Johnson, J., Rapin, W., Forni, O., & Wien, R. (2018). Chemical variability in mineralized veins observed by ChemCam on the lower slopes of Mount Sharp in Gale crater, Mars. *Icarus*, *311*, 69–86.

Malin, M. C., & Edgett, K. S. (2000). Sedimentary rocks of early Mars. *Science*, *290*, 1927–1937.

Mangold, N., Gendrin, A., Gondet, B., LeMouelic, S., Quantin, C., Ansan, V., & Neukum, G. (2008). Spectral and geological study of the sulfate-rich region of West Candor Chasma, Mars. *Icarus*, *194*, 519–543.

Martin, P. E., Farley, K. A., Baker, M. B., Malespin, C. A., Schwenzer, S. P., Cohen, B. A., et al. (2017). A two-step K-Ar experiment on Mars: Dating the diagenetic formation of jarosite from Amazonian groundwaters. *Journal of Geophysical Research: Planets*, *122*, 2803–2818. https://doi.org/10.1002/2017JE005445

Martin-Torres, F. J., Zorzano, M.-P., Valentin-Serrano, P., Harri, A.-M., Genzer, M., Kemppinen, O., & Vaniman, D. (2015). Transient liquid water and water activity at Gale crater on Mars. *Nature Geoscience*, *8*, 357–361. https://doi.org/10.1038/NGEO2412

McEwen, A. S., Eliason, E. M., Bergstrom, J. W., Bridges, N. T., Hansen, C. J., Delamere, W. A., & Weitz, C. M. (2007). Mars reconnaissance orbiter's high resolution imaging Science Experiment (HiRISE). *Journal of Geophysical Research*, *112*(E05S02). https://doi.org/10.1029/2005JE002605

McGuire, P. C., Bishop, J. L., Brown, A. J., Fraeman, A. A., Marzo, G. A., Morgan, M. F., & Wolff, M. J. (2009). An improvement to the volcano-scan algorithm for atmospheric correction of CRISM and OMEGA spectral data. *Planetary and Space Science*, *57*, 809–815.

Michalski, J. R., Cuadros, J., Bishop, J. L., Dyar, M. D., Dekov, V., & Fiore, S. (2015). Constraints on the crystal-chemistry of Fe/Mg-rich smectitic clays on Mars and links to global alteration trends. *Earth and Planetary Science Letters*, *427*, 215–225.

Milliken, R. E. (2011). *Mineralogy at Gale crater*. Talk given at the Fifth MSL Landing Site Workshop, Monrovia, CA. Retrieved from https://marsoweb.nas.nasa.gov/landingsites/landingsites.html

Milliken, R. E. (2020). *CRISM reflectance and geometry files processed with new methods described and used in "updated perspectives and hypotheses on the mineralogy of lower Mt. Sharp, Mars, as seen from Orbit"*, Providence, RI: Brown Digital Repository, Brown University Library. https://doi.org/10.26300/2q8p-wb51

Milliken, R. E., & Bish, D. L. (2010). Sources and sinks of clay minerals on Mars. *Philosophical Magazine*, *90*(17–18), 2293–2308.

Milliken, R. E., Ewing, R. C., Fischer, W. W., & Hurowitz, J. (2014). Wind-blown sandstones cemented by sulfate and clay minerals in Gale Crater, Mars. *Geophysical Research Letters*, *41*. https://doi.org/10.1002/2013GL059097

Milliken, R. E., Grotzinger, J. P., & Thompson, B. J. (2010). Paleoclimate of Mars as captured by the stratigraphic record in Gale crater. *Geophysical Research Letters*, *37*. https://doi.org/10.1029/2009GL041870

Murchie, S., Arvidson, R., Bedini, P., Beisser, K., Bibring, J.-P., Bishop, J., & Wolff, M. (2007). Compact Reconnaissance Imaging Spectrometer for Mars (CRISM) on Mars Reconnaissance Orbiter (MRO). *Journal of Geophysical Research*, *112*(E5), E05S03. https://doi.org/10.1029/2006JE002682

Murchie, S., Roach, L., Seelos, F., Milliken, R., Mustard, J., Arvidson, R., & Morris, R. (2009). Evidence for the origin of layered deposits in Candor Chasma, Mars, from mineral composition and hydrologic modeling. *Journal of Geophysical Research*, *114*, https://doi.org/10.1029/2009JE003343

Mustard, J. F., Murchie, S. L., Pelkey, S. M., Ehlmann, B. L., Milliken, R. E., Grant, J. A., & Wolff, M. (2008). Hydrated silicate minerals on Mars observed by the Mars Reconnaissance Orbiter CRISM instrument. *Nature*, 305–309.

Mustard, J. F., Poulet, F., Gendrin, A., Bibring, J. P., Langevin, Y., Gondet, B., & Altieri, F. (2005). Olivine and pyroxene diversity in the crust of Mars. *Science*, *307*, 1594–1597.

Nachon, M., Clegg, S. M., Mangold, N., Schroder, S., Kah, L. C., Dromart, G., & Wellington, D. (2014). Calcium sulfate veins characterized by ChemCam/Curiosity at Gale crater, Mars. *Journal of Geophysical Research: Planets*, *119*(9), 1991–2016. https://doi.org/10.1002/2013JE004588

Nachon, M., Mangold, N., Forni, O., Kah, L., Cousin, A., Wiens, R., & Sumner, D. (2017). Chemistry of diagenetic features analyzed by ChemCam at Pahrump Hills, Gale crater, Mars. *Sedimentology*, *281*, 121–136.

Pelkey, S. M., & Jakosky, B. (2002). Surficial geologic surveys of Gale crater and Melas Chasma, Mars: Integration of remote sensing data. *Icarus*, *160*, 228–257.

Pelkey, S. M., & Jakosky, B. (2004). Surficial properties in Gale crater, Mars, from Mars Odyssey THEMIS data. *Icarus*, *167*, 244–270.

Pelkey, S. M., Mustard, J. F., Murchie, S., Clancy, R. T., Wolff, M., Smith, M., & Gondet, B. (2007). CRISM multispectral summary products: Parameterizing mineral diversity on Mars from reflectance. *Journal of Geophysical Research*, *112*(E8). https://doi.org/10.1029/2006JE002831

Poulet, F., Bibring, J.-P., Langevin, Y., Mustard, J., Mangold, N., Vincendon, M., & Platevoet, B. (2009). Quantitative compositional analysis of Martian mafic regions using the MEx/OMEGA reflectance data. *Icarus*, *201*, 69–83.

Rampe, E., Ming, D., Blake, D., Bristow, T., Chipera, S., Grotzinger, J., & Thompson, L. (2017). Mineralogy of an ancient lacustrine mudstone succession from the Murray formation, Gale crater, Mars. *Earth and Planetary Science Letters*, *471*, 172–185.

Rapin, W., Ehlmann, B. L., Dromart, G., Schieber, J., Thomas, N. H., Fischer, W. W., & Vasavada, A. R. (2019). An interval of high salinity in ancient Gale crater lake on Mars. *Nature Geoscience*.

Rapin, W., Meslin, P.-Y., Maurice, S., Vaniman, D., Nachon, M., Mangold, N., & Archer, D. (2016). Hydration state of calcium sulfates in Gale crater, Mars: Identification of bassanite veins. *Earth and Planetary Science Letters*, *452*, 197–205.

Rice, M. S., Bell, I., Godber, A., Wellington, D., Fraeman, A. A., Johnson, J. R., & Grotzinger, J. P. (2013). *Mastcam multispectral imaging results from the Mars Science Laboratory investigation in Yellowknife Bay*. Paper presented at European Planetary Science Congress. London.

Rivera-Valentin, E. G., Gough, R. V., Primm, K. M., Martinez, G. M., Chevrier, V. F., & Tolbert, M. (2018). Constraining the potential liquid water environment at Gale crater, Mars. *Journal of Geophysical Research: Planets*, *123*, 1156–1167. https://doi.org/10.1002/2018JE005558

Roach, L. H., Mustard, J. F., Lane, M. D., Bishop, J. L., & Murchie, S. L. (2010). Diagenetic haematite and sulfate assemblages in Valles Marineris. *Icarus*, *207*, 659–674.

Roach, L. H., Mustard, J. F., Murchie, S. L., Bibring, J.-P., Forget, F., Lewis, K. W., & Bishop, J. L. (2009). Testing evidence of recent hydration state change in sulfates on Mars. *Journal of Geophysical Research*, *114*(E2). https://doi.org/10.1029/2008JE003245

Rossi, A. P., Pondrelli, M., van Gasselt, S., Zegers, T. E., Hauber, E., & Neukum, G. (2008). *Gale crater bulge: A candidate multi-stage large spring mound*. Abstract at the 39th Lunar and Planetary Science Conference, League City, TX.

Siebach, K. L., & Grotzinger, J. P. (2014). Volumetric estimates of ancient water on Mount Sharp based on boxwork deposits, Gale Crater, Mars. *Journal of Geophysical Research: Planets*, *119*(1), 189–198. https://doi.org/10.1002/2013JE004508

Stack, K. M., Edwards, C. S., Grotzinger, J. P., Gupta, S., Sumner, D. Y., Calef, F. J., III, et al. (2016). Comparing orbiter and rover image-based mapping of an ancient sedimentary environment, Aeolis Palus, Gale crater, Mars. *Icarus*, *280*, 3–21.

Stack, K. M., Sun, V. Z., Arvidson, R. E., Fedo, C., Day, M., Bennett, K., et al. (2019). *Origin of linear ridges in the clay-bearing unit of Mount Sharp, Gale crater, Mars*. Abstract at the 50th Lunar and Planetary Science Conference, The Woodlands, TX.

Stein, N., Grotzinger, J., Schieber, J., Mangold, N., Hallet, B., Newsom, H., & Dehouck, E. (2018). Desiccation cracks provide evidence of lake drying on Mars, Sutton Island member, Murray formation, Gale Crater. *Geology*, *46*(6), 515–518.

Sun, V. Z., Stack, K. M., Kah, L. C., Thompson, L., Fischer, W., Williams, A. J., & VanBommel, S. (2019). Late-stage diagenetic concretions in the Murray formation, Gale crater, Mars. *Icarus*, *321*, 866–890.

Sunshine, J. M., McFadden, L.-A., & Pieters, C. M. (1993). Reflectance spectra of the Elephant Moraine A79001 meteorite: Implications for remote sensing of planetary bodies. *Icarus*, *105*, 79–91.

Thomson, B., Bridges, N., Milliken, R., Baldridge, A., Hook, S., Crowley, J., & Weitz, C. (2011). Constraints on the origin and evolution of the layered mound in Gale crater, Mars using Mars Reconnaissance Orbiter data. *Icarus*, *214*, 413–432.

Tosca, N. J., McLennan, S. M., Dyar, M. D., Sklute, E. C., & Michel, F. M. (2008). Fe oxidation processes at Meridiani Planum and implications for secondary Fe mineralogy on Mars. *Journal of Geophysical Research*, *113*, E05005. https://doi.org/10.1029/2007JE003019

Vaniman, D. T., Bish, D. L., Chipera, S. J., Fialips, C. I., Carey, J. W., & Feldman, W. C. (2004). Magnesium sulphate salts and the history of water on Mars. *Nature*, *431*, 663–665.

Vaniman, D. T., Bish, D. L., Ming, D. W., Bristow, T. F., Morris, R. V., Blake, D. F., & Spanovich, N. (2014). Mineralogy of a mudstone at Yellowknife Bay, Gale crater, Mars. *Science*, *343*.

Vaniman, D. T., & Chipera, S. J. (2006). Transformations of Mg- and Ca-sulfate hydrates in Mars regolith. *American Mineralogist*, *91*, 1628–1642.

Vaniman, D. T., Martinez, G. M., Rampe, E. B., Bristow, T. F., Blake, D. F., Yen, A. S., & Sumner, D. Y. (2018). Gypsum, bassanite, and anhydrite at Gale crater, Mars. *American Mineralogist*, *103*, 1011–1020.

Viviano-Beck, C. E., Seelos, F. P., Murchie, S. L., Kahn, E. G., Seelos, K. D., Taylor, H. W., & Morgan, M. F. (2014). Revised CRISM spectral parameters and summary products based on the currently detected mineral diversity on Mars. *Journal of Geophysical Research: Planets*, *119*(6), 1403–1431. https://doi.org/10.1002/2014JE004627

Wang, A., Freeman, J. J., Jolliff, B. L., & Chou, I.-M. (2006). Sulfates on Mars: A systematic Raman spectroscopic study of hydration states of magnesium sulfates. *Geochimica et Cosmochimica Acta*, *70*, 6118–6135. https://doi.org/10.1016/j.gca.2006.05.022

Wang, A., Jolliff, B. L., Liu, Y., & Connor, K. (2016). Setting constraints on the nature and origin of the two major hydrous sulfates on Mars: Monohydrated and polyhydrated sulfates. *Journal of Geophysical Research: Planets*, *121*, 678–694.

Wiseman, S. M., Arvidson, R. E., Wolff, M. J., Smith, M. D., Seelos, F. P., Morgan, F., & McGuire, P. C. (2016). Characterization of artifacts introduced by the empirical volcano-scan atmospheric correction commonly applied to CRISM and OMEGA near-infrared spectra. *Icarus*, *269*, 111–121. https://doi.org/10.1016/j.icarus.2014.10.012

Wray, J. J. (2013). Gale crater: The Mars Science Laboratory/Curiosity rover landing site. *International Journal of Astrobiology*, *12*(1), 25–38.

Yen, A., Ming, D., Vaniman, D., Gellert, R., Blake, D., Morris, R., & Thompson, L. (2017). Multiple stages of aqueous alteration along fractures in mudstone and sandstone strata in Gale Crater, Mars. *Earth and Planetary Science Letters*, *471*, 186–198.